Check for updates

Network geometry

Marián Boguñá [1,2], *Ivan Bonamassa³, Manlio De Domenico* [4 ✉], *Shlomo Havlin³,*
Dmitri Krioukov [5,6,7,8] *and M. Ángeles Serrano* [1,2,9]

Abstract | Networks are finite metric spaces, with distances defined by the shortest paths between nodes. However, this is not the only form of network geometry: two others are the geometry of latent spaces underlying many networks and the effective geometry induced by dynamical processes in networks. These three approaches to network geometry are intimately related, and all three of them have been found to be exceptionally efficient in discovering fractality, scale invariance, self-similarity and other forms of fundamental symmetries in networks. Network geometry is also of great use in a variety of practical applications, from understanding how the brain works to routing in the Internet. We review the most important theoretical and practical developments dealing with these approaches to network geometry and offer perspectives on future research directions and challenges in this frontier in the study of complexity.

¹Departament de Física
de la Matèria Condensada,
Universitat de Barcelona,
Barcelona, Spain.

²Universitat de Barcelona
Institute of Complex Systems
(UBICS), Universitat de
Barcelona, Barcelona, Spain.

³Department of Physics,
Bar-Ilan University,
Ramat-Gan, Israel.

⁴CoMuNe Lab, Fondazione
Bruno Kessler, Povo, Italy.

⁵Network Science Institute,
Northeastern University,
Boston, MA, USA.

⁶Department of Physics,
Northeastern University,
Boston, MA, USA.

⁷Department of Mathematics,
Northeastern University,
Boston, MA, USA.

⁸Department of Electrical
and Computer Engineering,
Northeastern University,
Boston, MA, USA.

⁹ICREA, Barcelona, Spain.

✉e-mail:
mdedomenico@fbk.eu

https://doi.org/10.1038/
s42254-020-00264-4

Many existing analytical and computational tools for the analysis of complex networks emerged from classical methods in statistical physics[1]. Over the past two decades, these tools have proved essential for constructing models capable of reproducing the structural properties of many real-world networks[2–4]. They have also been used to quantify the importance of network structural properties for collective and critical phenomena[5–8]. Other fundamental insights have come from a variety of complementary approaches[9–13]. One such approach is geometry, the focus of this Review Article.

The first evidence that complex networks possess some non-trivial geometric properties appeared with the discovery of their self-similarity under suitable scale transformations[14]. Initially, fractal geometry was a major reservoir of methods and ideas. Besides boosting the study of transport phenomena in complex media[15,16], the fractal geometric paradigm led to the definition of a reversible graph-theoretical renormalization procedure that helped researchers classify networks into universality classes[17,18] and to better understand the growth mechanisms underlying their temporal evolution[19].

Following the lines of this initial success, it was later found[20] that network self-similarity can be explained at a more fundamental level in terms of latent hyperbolic geometry[21]. Latent spaces have been employed for nearly a century to model homophily in social networks[22–24]. In these models, nodes are positioned in a similarity space. Connections between them are random, but they are the more likely the closer the two nodes in the space, that is, more similar nodes are more likely to be connected. This approach, with the latent space taken to be hyperbolic, is the basis for a unified framework that explains the most common structural properties of many real networks[20,21],

their navigability[25–28], and their community[29–33] and multiscale[34] structures. Because the group of symmetries of hyperbolic spaces is isomorphic to the Lorentz group, the latent hyperbolicity of networks was advocated to explain not only their structural self-similarity but also the dynamical laws of their growth[35–37]. The isomorphism also establishes certain duality relations[38] reminiscent of the anti-de Sitter/conformal field theory correspondence in theoretical physics.

In light of these advances, it is not surprising that the geometric approach led to many practical applications and theoretical insights. For example, in the context of information or epidemic spreading, the adoption of transport-based metrics and of the corresponding diffusion geometries[39] is helping explain the spatiotemporal evolution of network-driven dynamical processes[40,41], opening new research directions[42,43] in many neighbouring areas of science.

The rapid evolution of research areas related to network geometry has led to cross-fertilization among many areas of science. This rapid interdisciplinary progress suggests that now is an apt time to ground a milestone in network geometry research, from where to ponder future challenges. We review three major research directions in network geometry: the self-similar fractal geometry of network structure, the hyperbolic geometry of networks' latent spaces and the geometry induced by dynamical processes, such as diffusion, in networks. Distances are all different in the three geometries, yet intimately related. In fractal geometry, distances are the shortest-path distances, that is, the hop lengths of shortest paths in a network. In latent geometries, distances are the distances between network nodes in a latent space. In geometry induced by dynamical

Key points

- The fractal geometry of networks enables casting the self-similar symmetries underlying the organization of complex systems under the three pillars of scaling, universality and renormalization.
- Latent metric spaces with hyperbolic geometry provide a natural explanation for the architecture of real complex networks, including small-worldness, degree heterogeneity, clustering, community structure, symmetries and navigability.
- Multiscale unfolding of complex networks is possible by means of a geometric renormalization technique that uncovers self-similarity at different scales.
- Network dynamical processes induce kinematic distances that characterize an effective geometry of a system's function, which cannot be obtained by purely topological latent geometry.
- Network geometry enhances our understanding of complex systems across their multiple scales of organization and of collective phenomena emerging from their information exchange.

processes, distances are the kinematic distances, such as those emerging from spreading dynamics in a network such as reaction–diffusion or random-search processes. We discuss open questions and future challenges, relating to both theory and applications of these three flavours of network geometry.

Understood broadly, network geometry encompasses diverse research directions, many of which are as important as the ones covered here, thus deserving separate reviews. Therefore, in a short Review Article like this one, most of these directions must unfortunately be omitted. The most notable omissions include spatial networks, quantum gravity, graph curvature, geometrogenesis, graph embedding, topological data analysis, topological graph theory and Gromov's δ-hyperbolicity. However, in the outlook we briefly comment on some of these topics that we find particularly important, promising or intriguing.

Fractal geometry of network structure

Many natural objects are best described geometrically as fractals[44], with self-similar patters on all their available length scales and well-defined fractal dimensions. From surfaces and snowflakes to turbulent flows[45] or critical phenomena near phase transitions[46,47], this scale-free property is among the basic hallmarks of complexity, reflecting certain laws and organizing principles[48,49] underlying nature's evolution.

The discovery of the scale-free nature of many real networks has added a new paradigm to this understanding, providing scientists with a versatile proxy to tame complexity on combinatorial grounds[50]. In this context, scale-freeness refers to the absence of a characteristic number of links k per node (rather than a length scale), as described by a fat-tailed degree distribution of the form $P(k) \sim k^{-\gamma}$ as $k \gg 1$, with the scale-free exponent $\gamma \in (2, 3)$. This scale-free property hinted at the existence of some degree of structural invariance under a suitable rescaling. However, the equally ubiquitous small-world[2] property — that is, an average distance between nodes growing logarithmically or slower[51–53] with the system size N — contextually hindered this possibility, implying a diverging Haussdorf dimension. This led to the common belief that networks cannot be self-similar. Fortunately, this apparent contradiction

proved to be a problem that prompted prolific research, and its analysis through tools of fractal geometry[54] has disclosed fundamental insights into the hidden symmetries, renormalization and universality classes of complex networks.

Shortest-path-distance scaling and dimensions. The number ℓ of edges along any shortest path connecting two nodes is a well-defined metric[55]. It is known as the shortest-path distance (or, sometimes, chemical distance)[56,57], and it can be adopted to observe networks at different length scales. The process of zooming out on networks can be performed analogously to that on ordinary fractals by repeatedly coarse-graining the structure through optimal coverings of nodes made by non-overlapping boxes of diameter ℓ_B (BOX 1)[14]. Under this renormalization group (RG) transformation[58,59], a surprising variety of real-world and synthetic networks remain statistically self-similar, in the sense that their degree distribution[14] and other mixing patterns[60] are invariant (FIG. 1a) over the available length scales.

A primary consequence of the discovery of networks' self-similarity was their characterization through a set of fractal dimensions[61] intimately related to their multiscale organization and functioning. In what follows, we review an essential selection of these network dimensions and their significance.

We start from two crucial quantities: the number of boxes (supernodes) N' optimally covering a network and the degree sequence $\{k_i'\}_{i=1,...,N'}$ of the boxes, where each k' corresponds to the degree of the hub contained in the 'parent' box. Performing a shortest-path-distance RG transformation step, $\mathcal{R}_B$, these quantities have power-law scaling (FIG. 1a)

$$N \overset{\mathcal{R}_B}{\to} N' \sim \ell_B^{-d_B} N, k \overset{\mathcal{R}_B}{\to} k' \sim \ell_B^{-d_k} k. \qquad (1)$$

The exponents (d_B, d_k) are the box and degree dimensions, respectively (FIG. 1b, top and middle panels); they characterize the (RG invariant) scale-free degree distribution through the scaling identity $\gamma = 1 + d_B/d_k$ (REF.[14]). Besides unveiling a fundamental connection between scale-free and RG-invariant properties, this fractal analysis yields a birds-eye view over the spectrum of different organization mechanisms that underlie self-similar networks. It does so by identifying two limiting cases[62,63]: fractal structures when d_B and d_k are both finite and non-zero (in biological systems, the world wide web (WWW) or social networks, for example), and small worlds when $d_B, d_k \to \infty$ (in the Internet at the router level or synthetic networks, for example), implying an exponential decay in the N and k distributions (FIG. 1b, top panel) instead of the scaling of equation 1.

A more comprehensive picture is reached by analysing structural fractality in terms of the profiles of degree–degree correlations[14,64]. Fractal networks feature a strong 'hub–hub repulsion', which leads to disassortative structures, with hubs spread uniformly instead of being crumpled in a core as they are in pure small worlds. In light of their RG invariance[60], these correlation

patterns can be captured by a hub–hub dimension d_e, defined by the scaling factor $\mathcal{E}(\ell_B) \sim \ell_B^{-d_e}$, which is proportional to the probability that two RG boxes are connected through their hubs (FIG. 1b, bottom panel). Scaling arguments analogous to those adopted for the triple (d_B, d_k, γ) make it possible to relate the correlation exponent $\varepsilon > 1$ — defined by the RG invariant[60] degree–degree distribution $P(k, q) \sim k^{-\gamma+1}q^{-\varepsilon}$ — to the hub–hub dimension through the identity $\varepsilon = 2 + d_e/d_k$ (REF.[60]). These results allow the classification of many networks according to RG-invariant properties related to their large-scale organization (FIG. 1c).

A final essential feature of the fractal geometry of networks is the existence of a larger group of self-similar symmetries that leave invariant the network mesoscale organization. In fact, the RG transform identifies a hierarchy of modular configurations into which networks can be optimally partitioned at increasing length scales. The scale invariance of such a tiling can be quantified via the power-law scaling $\mathcal{Q}(\ell_B) \sim \ell_B^{d_M}$ (REFS[15,65]), where d_M is the modular dimension and $\mathcal{Q}(\ell_B)$ is a modularity factor[66,67] maximized by the box covering. The value $d_M = 1$ (characterizing regular lattices) is the border line between modular structures ($d_M > 1$, typical of biological networks, for instance) and non-modular ones ($d_M < 1$); networks with lower values of d_M are more small-world-like. We will see in what follows that d_M, unlike the other 'structural' dimensions, is

---

Box 1 | Zooming out on complex networks

Shortest-path-distance renormalization

In the box-covering technique (see the figure, part **a**), the original network (first column) is tiled with the minimum number of boxes of diameter ℓ_B — using the maximum excluded mass burning algorithm[272], for instance — which are contracted into supernodes (second column) and then connected though at least one link existed between the 'parent' tiles. This coarse graining is repeatedly applied — albeit for a limited number of steps due to small-worldness — until the network is reduced to a single 'ancestral' node. As an example, the shortest-path-distance renormalization group can be applied to the entire world wide web, here with with $\ell_B = 2$ (see the figure, part **b**). The network's structure remains statistically invariant under the renormalization (FIG. 1).
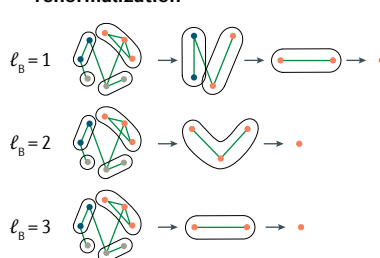
Degree-thresholding renormalization

Subgraphs are obtained by removing all nodes with degrees below a given threshold k_T (see the figure, part **c**). Doing so defines a hierarchy of nested subgraphs that in real complex networks are found to be self-similar. Applying this procedure to the Internet border gateway protocol (BGP) graphs (see the figure, part **d**, left column) and its randomized version that preserves the degree sequence (see the figure, part **d**, right column) shows that the clustering spectrum (average clustering coefficient $\bar{c}$ versus rescaled internal degree $k_i/\langle k_i(k_T)\rangle$) exhibits data collapse for the original network but not for the randomized network. The nice collapse of the clustering spectrum for real complex networks finds a natural explanation in their underlying geometry[20].
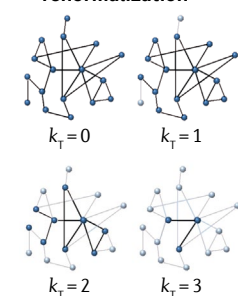
Geometric renormalization

Like shortest-path renormalization, the geometric renormalization transformation zooms out by changing the minimum length scale from that of the original network to a larger value, this time in the similarity space[34] (see the figure, part **e**). For each layer l of the renormalization transformation, first, non-overlapping blocks of consecutive nodes are defined along the similarity circle. Second, the blocks are coarse-grained into supernodes. Each supernode is then placed within the angular region defined by the corresponding block so that the order of nodes is preserved. Finally, two supernodes are connected if any of their constituents were in the precursor layer. This procedure has been performed on the hyperbolic embedding of the human metabolic network and its renormalized layer $l = 2$ (REF.[34]; see the figure, part **f**). The colours of the nodes correspond to the community
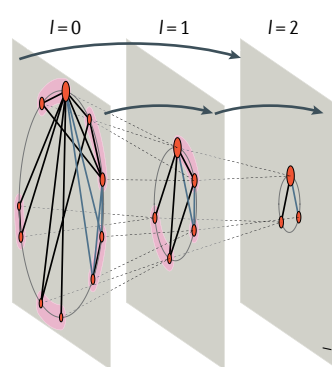
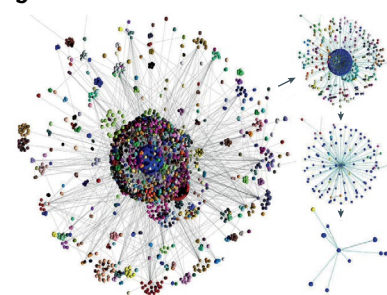**a Shortest-path-distance renormalization**

$\ell_B = 1$

$\ell_B = 2$

$\ell_B = 3$

b

c Degree-thresholding renormalization

$k_T = 0$ $k_T = 1$

$k_T = 2$ $k_T = 3$

d

Internet BGP map

Internet BGP map randomized

$\bar{c}(k_i/k_T)$

$k_i/<k_i(k_T)>$

$\bullet k_T = 5$ $\blacksquare k_T = 10$ $\blacklozenge k_T = 20$ $\blacktriangle k_T = 50$ $\blacktriangledown k_T = 100$

e Geometric renormalization

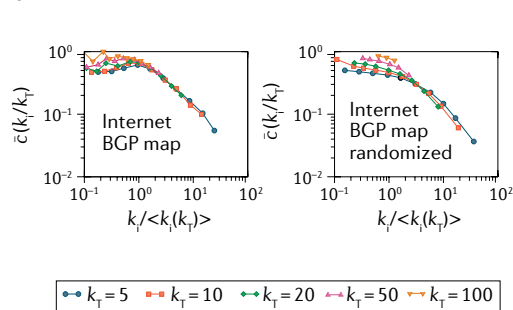$l = 0$ $l = 1$ $l = 2$

f
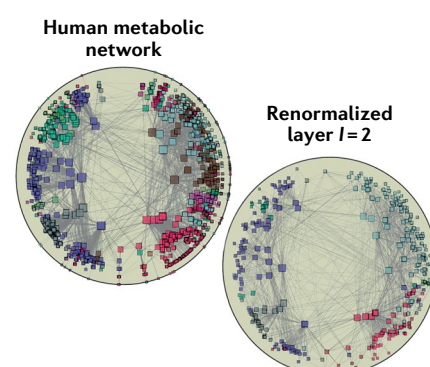
Human metabolic network
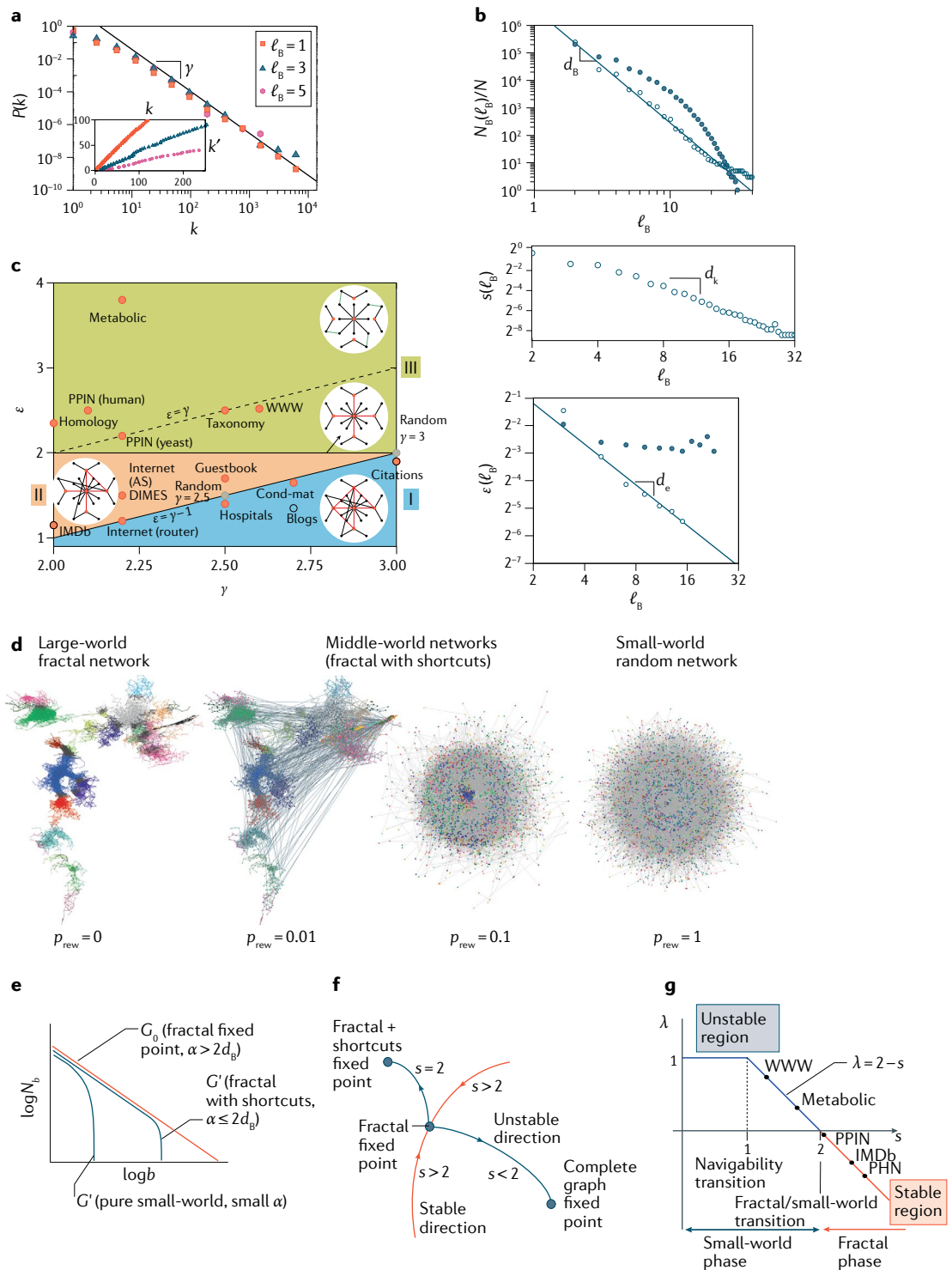
Renormalized layer $l = 2$

structure detected by the Louvain algorithm[273]. The renormalized network preserves the original community structure despite being four times smaller.

Parts **a,b** reprinted from REF.[14], Springer Nature Limited. Parts **c,d** adapted with permission from REF.[20], American Physical Society. Parts **e,f** adapted from REF.[34], Springer Nature Limited.

directly connected to other dynamical exponents that characterize transport in complex media.

RG flow. Repeatedly applying the shortest-path-distance RG transformation, $\mathcal{R}_B$, identifies a flow in the space of graph configurations. Much like the case of critical phenomena[58,59,68], such a flow enables a classification of network topologies into universality classes. Indeed, scale invariance and self-similarity are natural symmetries featured by the fixed points of the RG flow, whose

stability against small perturbations enshrines universal features.

A generalization of finite-size scaling methods[17] has been used to analyse the RG flow beyond the limiting constraint of a few RG steps, a constraint that arises because of the networks' small-worldness. For a large set of real-world and artificial networks[69], a coherent picture about their stability under the RG flow emerged after looking at the critical exponents governing their fluctuations (γ') and correlation length (ν)[70].

Fig. 1 | **Structural self-similarity, renormalization-group flow and universality.**
a | Renormalization group (RG) invariance of the world wide web (WWW) degree
distribution $P(k) \sim k^{-\gamma}$ (γ is the scale-free exponent) and of its degree sequence ($k' \sim \ell_B^{-d_k} k$,
see equation 1) for different box diameters ℓ_B (inset). **b** | RG scaling factors of box sizes
$N_B(\ell_B)/N$ (N_B is the number of boxes and N the number of nodes) (top), their degree
sequence $s(\ell_B) \equiv k'/k$ (middle) and the hub–hub correlations $\mathcal{E}(\ell_B)$ (bottom). Fractal
networks (such as the WWW, open circles) feature well-defined dimensions d_B, d_k and d_e;
non-fractal ones (such as the Internet, filled circles) show an exponential (or faster) decay,
that is, d_B, $d_k \to \infty$ and $d_e \to 0$. **c** | Classification of self-similar networks in the (γ, ε) plane
(ε is the correlation exponent). At the line $\varepsilon = \gamma - 1$, the network structure is random. Below
the line (region I), hub correlations are stronger than in random networks; above the line,
hub correlations are weaker than random. The scaling identity $\varepsilon = 2 + d_e/d_k = 2 + (\gamma - 1)d_e/d_B$,
for which $d_B \to \infty$ yields $\varepsilon = 2$, distinguishes non-fractal (region II) from fractal networks
(region III). Within region III, the subregion defined by $\varepsilon \geq \gamma$ identifies the realm of
hierarchical scale-free graphs. A description of the databases and acronyms used can be
found at http://jamlab.org. **d** | Fractal to small-world transition, obtained by randomly
rewiring a fraction p_{rew} of links. Whereas modularity is rapidly lost, small-worldness is
rapidly gained, emphasizing the trade-off between these network phases. **e** | Crossover
from the power-law scaling to an exponential decay in fractal networks upon the random
addition of shortcuts according to the probability $P(\ell) \sim \ell^{-\alpha}$. All N_b nodes within a box are
within a shortest-path distance $\leq b$. **f** | RG flow diagram in the space of configurations.
In the stable phase ($s \equiv \alpha/d_B > 2$), the RG flows towards the fractal fixed point, whereas in
the unstable phase ($s < 2$) it flows towards a complete graph. For $s \approx 2$, the scaling has an
exponential cut-off at a characteristic scale (part **e**): globally the network is small world
and at small scales it is fractal. **g** | Stability analysis of the RG flow (in terms of stability
exponent λ) leads to equations 2 and 3. A navigability transition exists at $s = 1$ and
a fractal to small-world transition at $s = 2$. Real-world networks can be classified
accordingly. See REF.[18] for additional information regarding the databases used and
their corresponding acronyms. Part **a** reprinted from REF.[14], Springer Nature Limited.
Part **b** (top) adapted with permission from REF.[85], Elsevier; (middle) adapted from REF.[75],
Springer Nature Limited; (bottom) adapted from[19], Springer Nature Limited. Part **c**
adapted with permission from REF.[60], American Physical Society. Part **d** adapted with
permission from REF.[83], PNAS. Parts **e**–**g** reprinted with permission from
REF.[18], American Physical Society.

All small-world networks, such as Erdős–Rényi graphs,
Watts–Strogatz networks or the preferential attachment
model, are characterized by $\nu = \gamma' = 2$. Conversely, frac-
tal structures, such as the Song–Havlin–Makse (SHM)
model, Apollonian networks or percolating clusters,
feature different values of ν and γ'. The SHM model[15,19]
is generated by a multiplicative process of network
growth, the dynamics of which follow the inverse of the
shortest-path-distance RG transform. For this model,
in particular, $\nu = \gamma' = 1$ for every scale-free exponent,
whereas $\nu = \gamma' = 2$ after any arbitrarily small random
rewiring[69], suggesting that fractal topologies are indeed
unstable fixed points of the shortest-path-distance
RG flow. For increasing fractions of randomly drawn
shortcuts, in fact, fractal networks rapidly cross over to
more and more compact architectures (FIG. 1d) that have
weaker and weaker modularity. This crossover leads to
networks with fractal scaling $\bar{\ell} \sim N_0^{1/d_B}$ that is observed
only up to a certain cut-off length scale before a global
small-world behaviour $\bar{\ell} \sim N_0^{1/d_B}$ is found (FIG. 1e).

These promising results prepared the ground for the
firm RG theory presented in REF.[18], which elucidates
the universal features underlying the fractal to small-
world transition in complex networks. Adding short-
cuts to a fractal network G_0 with a probability $p(\ell) = \mathcal{A}$
$\ell^{-\alpha}$, where $\mathcal{A}$ is a normalization constant, causes the RG
trajectories to either converge towards G_0 or to transform
the network into a complete graph — a trivially stable
fixed point of the RG flow — depending on the value of

the exponent $\alpha > 0$. These outcomes can be quantified by
focusing on the renormalized distribution of shortcuts
after one RG step, which, in the formal limit of $\ell_B \to \infty$,
leads to the fixed point equation

$$p^*(\ell) \equiv 1 - \lim_{x \to \infty} \exp[-C(\ell)x^{2d_B/\alpha - 1}], \qquad (2)$$

where $C(\ell) \equiv \mathcal{A}^{2d_B/\alpha} \ell^{-2d_B}$ and $x \equiv \mathcal{A}^{-1}(\ell_B\ell)^{\alpha}$. Equation 2
has three distinct solutions (FIG. 1f), depending on the
value of the parameter $s \equiv \alpha/d_B$:
- if $s > 2$, then $p^*(\ell) = 0$ and the RG flow converges again
  towards the fractal network G_0;
- if $s < 2$, then $p^*(\ell) = 1$ and the RG flow converges
  towards the complete graph fixed point;
- if $s = 2$, then the RG flow has one non-trivial stable
  fixed point G', consisting of G_0 dressed with shortcuts
  following $p^*(\ell) = 1 - \exp(-\mathcal{A}\ell^{-2d_B})$.

Analysing the flow of the difference between the
average degree z_0 in G_0 and the average degree z_B in
the renormalized network $G_B = \mathcal{R}_B(G')$ yields further
insights into these three network phases. Such analysis
shows that $z_B - z_0 = (z' - z_0)\mathcal{D}(x_B)$ where, in the thermo-
dynamic limit, the function $\mathcal{D}(x_B)$ scales with the rela-
tive network size as $\mathcal{D}(x_B) \sim x_B^{\lambda}$ and the RG exponent
λ depends on the shortcut exponent α as

$$\lambda = \begin{cases} 1, & \text{if} \quad s \leq 1, \\ 2 - s, & \text{if} \quad s > 1. \end{cases} \qquad (3)$$

Equation 3 identifies two transitions in the space of
network configurations (FIG. 1g). One is a small-world-to-
fractal transition at $s = 2$, equivalently at $\alpha = 2d_B$, separat-
ing the stable ($\lambda < 0$, $s > 2$) phase of compact topologies
from the unstable phase ($\lambda > 0$, $s < 2$) of modular struc-
tures. The other transition is a navigability transition
at $s = 1$, equivalently at $\alpha = d_B$, which is the network
analogue of Kleinberg's optimal point[71].

Besides raising theoretical questions regarding the
characterization of these configurational transitions,
the RG theory sketched above provides an indirect
method for extracting information about the distri-
bution of shortcuts in fractal real-world networks —
a crucial ingredient for understanding information
flow and optimal search[72] — and for determining their
approximate location in the space of network config-
urations. Such analysis has been applied to the WWW,
the metabolic network of *Escherichia coli*, a yeast protein–
protein interaction network, the actors network of the
Internet Movie Database and the protein homology
network (FIG. 1g). The results show, in particular, that the
WWW (FIG. 1b) is fractal up to a given length scale, but it
is also sufficiently randomized to host an optimal flow,
as manifested by its proximity in the (λ, s) plane to the
navigability threshold.

Network functionality and evolution. Although the
shortest-path-distance RG placed the mixing patterns
of networks (such as the degree distribution) on more
fundamental grounds, it also raised several puzzles of
interpretation[73]. Questions arose about the functional
significance encoded in the modules detected by the RG.

Furthermore, it soon proved impossible to understand their emergence in terms of popular mechanisms of network growth[74], such as the 'rich get richer' principle of preferential attachment, or the 'democratic' wiring of Erdős–Rényi networks, which are generally dominated by small-worldness.

The first issue was soon clarified by analysing biological networks[15,19,65], for which the RG transform has led to identification of hierarchies of modules closely related to their known biochemical annotations, with a resolution as accurate as that of other clustering algorithms[4,66,67]. An important example of what RG analysis has enabled is an integrated multiscale view of the network of human cell differentiation[65], raising the possibility of identifying hitherto unknown functional relations between previously unrelated cellular domains.

The problem of growth, instead, has been elegantly solved by building on the observation that modular networks are also fractal (though the converse is not necessarily true). The SHM model (FIG. 2a,b) is built on this property[15,19]. In this model, hubs acquire new connections by linking preferentially with less connected nodes, subject to the noisy appearance (as exemplified in the Watts–Strogatz model) of randomly placed shortcuts. The net result is that hubs are buried deep in modules whose low-degree nodes are the inter-module connectors, resulting in scale-free networks that are fractal and modular up to a cut-off scale above which they become global small worlds (FIG. 1e). The SHM model represents a theoretical benchmark for understanding the self-similar patterns observed in real-world systems in terms of the microscopic growth rates controlling their dynamics[75], and it has raised important evolutionary implications. Besides highlighting the evolutionary drive of many biological networks[19] towards fractal modular structures — which maximize their robustness against random failures[76] — the SHM model has been used to reveal the inherently fractal geometric nature of the duplication-divergence mechanisms in genetics, suggesting that fractality and multiplicative growth are essential features of the evolution of biological networks. A notable result in this respect is the successful reconstruction of the present-day structures of several protein–protein interaction networks (FIG. 2c),
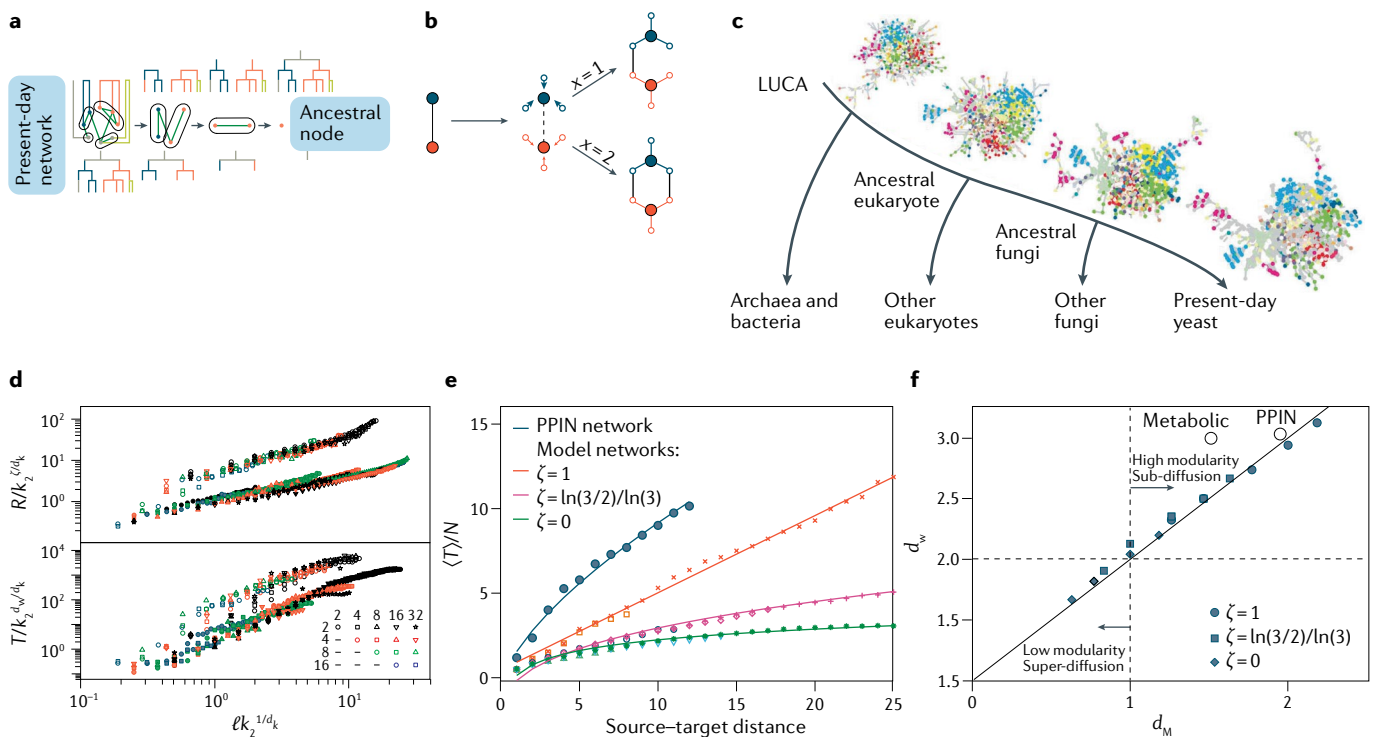

Fig. 2 | **Network evolution and transport theory. a** | Dendrograms demonstrating the network evolution (top tree) as inverse of the shortest-path-distance renormalization group (RG) procedure (bottom tree) (BOX 1). The arrow of time increases from right to left. **b** | Seeds of the Song–Havlin–Makse (SHM) model for network growth. At each time step, a node produces m offspring for every link. The original link is then removed with probability e, and x new links between randomly selected nodes of the new generation are added. Illustration: $m = 3$ and $e = 1$. e tunes between pure fractals ($e = 1$) and pure small worlds ($e = 0$) and x controls the degree of modularity, so that $x = 1$ yields tree-like structures and shortcuts among modules appear for $x > 1$. **c** | Phylogenetic tree showing the evolutionary path of the *Saccharomyces cerevisiae* protein–protein interaction network (PPIN), reconstructed from the last universal common ancestor (LUCA) to its present-day structure by combining the SHM growth model with the RG process. Colours represent functional categories. **d** | Data collapse of the resistance R (top) and the diffusion time T (bottom) according to equation 4 for the yeast PPIN (open symbols) and the SHM model with $e = 1$ (filled symbols). Markers indicate ratios of scaling parameters k_1/k_2, and colours denote values of k_1. d_w, walk dimension; d_k, degree dimension; ζ, conductivity dimension. **e** | Comparison between the finite-size scaling law equation 5 and simulated diffusion times normalized by the network size N (markers) in the PPIN and SHM model with $m = 3$ and $e = 1$. **f** | Modularity versus transport in real-world and SHM model networks in the (d_w, d_M) plane (d_M is the modular dimension). Part **a**, adapted with permission from REF.[85], Elsevier. Part **c** is adapted from REF.[77], CC BY 4.0. (https://creativecommons.org/licences/by/4.0/). Part **d,f** adapted with permission from REF.[15], PNAS. Copyright (2007) National Academy of Sciences, U.S.A. Part **e** adapted from REF.[16], Springer Nature Limited.

starting from their primitive ancestors identified via the shortest-path-distance RG technique[77].

Transport in self-similar media. Discovering the fractal geometry of networks has also had implications for the study of transport in complex media, a notoriously hard theoretical problem[78]. In fact, the existence of an underlying self-similar symmetry makes it possible to circumvent the search for exact solutions and to attack the problem by means of scaling arguments. A first result in this direction[15] involved the scale-invariant forms featured by the mean diffusion time, $T \sim \ell^{d_w}$, and the average resistance, $R \sim \ell^{\zeta}$, experienced by a blind ant travelling a shortest-path distance ℓ, where d_w is the walk dimension and ζ is the conductivity dimension[79] of the underlying medium. Combining these relations with equation 1, the observables T and R re-scale as $T'/T \sim (N'/N)^{d_w/d_B}$ and $R'/R \sim (N'/N)^{\zeta/d_B}$ under RG transformations. A direct evaluation of d_w and ζ in biological and synthetic (SHM) networks with with finite d_B reveals[15] that d_B, d_w and ζ obey the Einstein identity[80] $\zeta = d_w - d_B$, elegantly relating static and dynamic properties of transport in complex media. Thanks to this insight, it proved possible to predict the dependence of T and R on microscopic network features — such as nodes' degrees and the shortest-path distance between them — leading to the scaling relations

$$T(\ell; k_1, k_2) = k_2^{d_w/d_k} f_T \left(\ell / k_2^{1/d_k} \right),$$
$$R(\ell; k_1, k_2) = k_2^{\zeta/d_k} f_R \left(\ell / k_2^{1/d_k} \right),$$

$$(4)$$

where $f_{T,R}$ are scaling functions. These scaling relations agree well with the collapse of real-world networks data (FIG. 2d). Furthermore — and more completely than the above scenario — the assumption of self-similarity has been used to develop a general theory of transport in complex media[16]. This theory culminates in the exact finite-size expression

$$T(\ell) \sim \begin{cases} N(a + \text{sgn}(\zeta)b\ell^{\zeta}), & \zeta \gtrless 0, \\ N(a + b\ln \ell), & \zeta = 0, \end{cases}$$

$$(5)$$

where a and b are positive constants. Equation 5 describes a universal scaling law for transport in complex media[81] with finite d_B (FIG. 2e).

Besides their importance for theory, these results have offered new methods of fractal geometry to relate the kinetics of transport-limited processes in real-world systems to their interaction topologies. In particular, equation 4 enables bridging of the degree of modularity of networks to their efficiency of transport[15]. This relationship is epitomized by the identity $d_w = 1 + d_M$ (FIG. 2f): high levels of modularity ($d_M > 1$) generally result in subdiffusive dynamics ($d_w > 2$). This simple result has had significant implications in applications such as the characterization of the flux responses of metabolites[15] or the community detection in global small-world social networks[82], and it has provided intriguing ideas for addressing the long-standing conundrum of the highly modular yet globally optimal organization of functional brain networks[83,84].
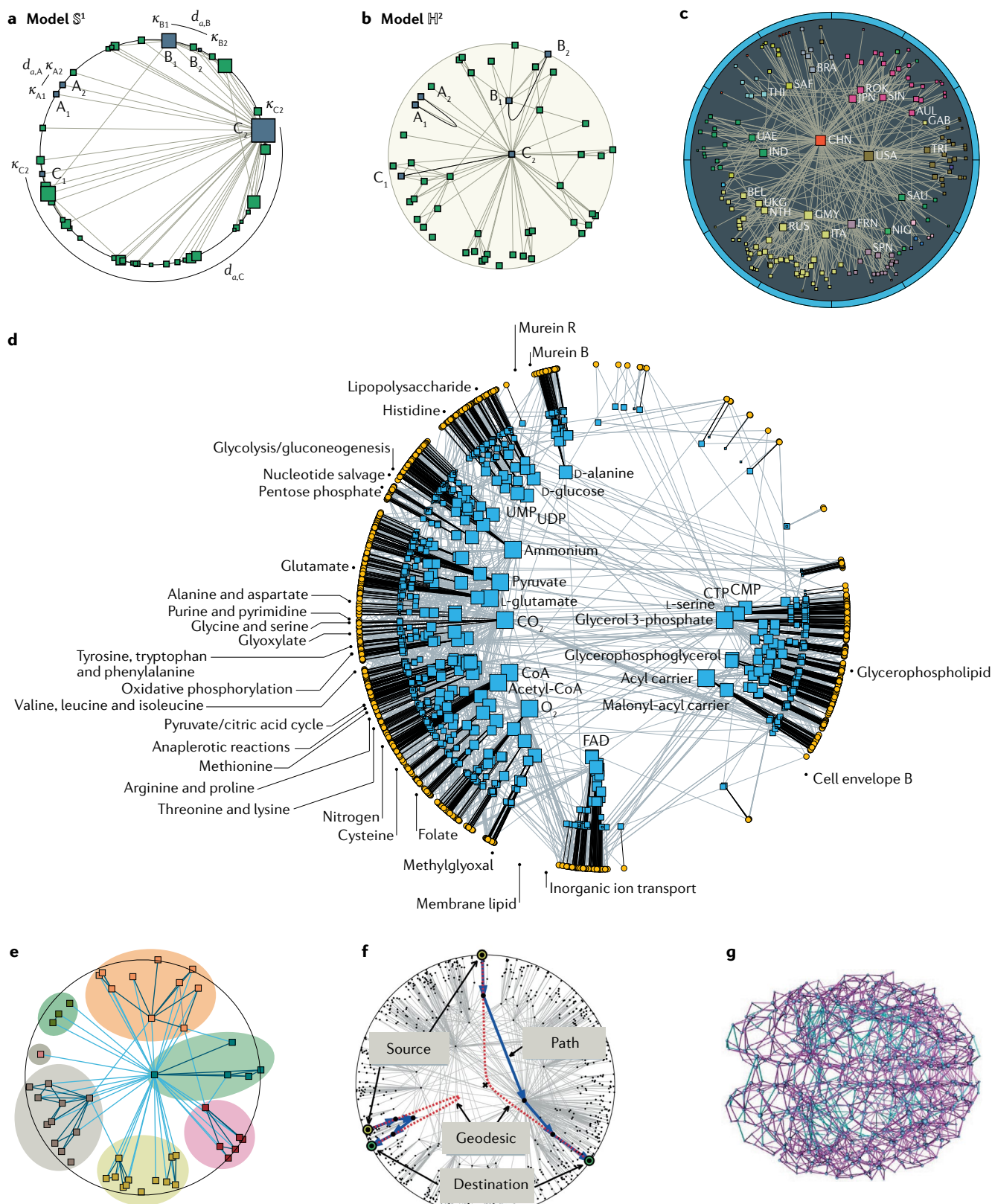
Open questions. One pragmatic question raised by the fractal geometry of network structures involves the very same notion of self-similarity and fractality in complex networks. Although traditional fractal theory does not distinguish between fractality and self-similarity, these two properties are distinct under the lens of the shortest-path-distance RG[85]. Whereas both fractal and pure small-world structures are statistically self-similar under the shortest-path-distance RG (see, for example, Fig. S6 in REF.[19] and discussions therein), only the fractal structures feature a well-defined set of (finite) fractal exponents. The divergence of d_B in small-world networks (FIG. 1b) can be interpreted (using field theory jargon) as an 'ultraviolet' limit above which the fractal geometric approach based on the shortest-path RG fails to quantify the self-similar symmetry. In this perspective, identifying suitable embeddings or duality transformations[86] that can regularize this 'small-world divergence' is an open theoretical challenge that could raise the opportunity of designing a unified geometric framework for the study of fundamental problems such as transport[78], evolution[37], navigability[25] or RG-based classification of the universality classes of networks[18]. In this respect, latent-geometric approaches or the adoption of generalized topological metrics and embeddings[87] could offer hints for solutions. Hyperbolic geometry, in particular, shares profound connections with self-similar metric spaces[88–90], suggesting the possibility that the fractal exponents featured by self-similar networks may have suitable counterparts in their corresponding latent spaces and could further be extended to pure small-world structures.

On a more fundamental level, understanding how the dynamical properties of network growth processes influence their asymptotic self-similar patterns is an intriguing and as yet unexplored territory in the study of network geometry. The process of zooming out induced by the network RG transform finds its (statistically equivalent) inverse in dynamics[19,37], so that the varying structures observed at increasing length scales correspond to the evolution of certain dynamical variables (FIG. 2a). A profound link between self-similarity and ergodicity has been explored in mathematics[91], showing that the notions of fractal dimensions and self-similarity can be interpreted in terms of ergodic averages of some appropriate measure-preserving dynamical systems[92]. In the simple case of growing trees, it has further been proved[91] that this connection is a consequence of the explicit dependence of the fractal dimension on the growth rates ruling the system's evolution. An analogous result holds for the self-similar structure of the SHM model in the thermodynamic limit[19]: its characteristic fractal exponents d_B, d_k, d_M, ... depend only on the process' growth rates (FIG. 2b). A relevant and challenging question, in this respect, is to understand weather the SHM model and/or other more popular growth processes[19,37,93] can be themselves interpreted as ergodic dynamical systems with respect to some suitable invariant measure. Besides its theoretical relevance, finding viable directions to tackle this overarching problem could help establish fundamental connections among the static and dynamic facets of network geometry.

Hyperbolic geometry of latent spaces

Deep connections between self-similarity and hyperbolic geometry have been well explored by mathematicians[88,90,94]. One connection goes via the observation that any Gromov-hyperbolic space has a boundary at infinity that is always a self-similar metric space[94]. Another connection is that self-similar groups can always be represented as the groups of automorphisms of trees, which are the simplest example of discrete hyperbolic spaces[90]. The connections between

a   Model $\mathbb{S}^1$

b   Model $\mathbb{H}^2$

c

d

e

f

g

hyperbolicity and self-similar sets, fractals and similar objects also go through the idea that rescaling is (approximately) an isometry transformation in (coarse) hyperbolic geometry[95].

Yet hyperbolic geometry is not the geometry of the observable structure of real-world networks discussed above, but the geometry of their latent spaces that we discuss here. The two geometries are intimately related because network paths that follow hyperbolic geodesics in the latent space are the shortest paths in the network with high probability[21,25,96,97] — the network is said to be congruent with its underlying latent geometry.

Models. Models in which nodes are connected based on their proximity in a latent space are known as (soft) random geometric graphs in mathematics, where they have been extensively explored[98]. In the simplest random geometric graph model, n nodes are placed uniformly at random on the interval $[0, n]$ with periodic boundary conditions, that is, on the circle $\mathbb{S}^1$. The node pairs are then connected if the distance between them on the circle is less than a parameter $\mu > 0$ controlling the average degree ($\langle k \rangle = 2\mu$). The model yields networks with non-vanishing clustering ($\langle c \rangle = 3/4$) and an average shortest-path length that scales linearly with network size. Such networks are thus large worlds.

From the statistical physics perspective, this simplest possible latent-space network model is the zero temperature (that is, the inverse temperature $\beta \to \infty$) limit of a more general entropy-maximizing probabilistic mixture of grand canonical ensembles with the Fermi–Dirac probability of connection between nodes i and j:

$$p_{ij} = \frac{1}{e^{\beta(\varepsilon_{ij} - \mu)} + 1}. \tag{6}$$

◀ Fig. 3 | **Networks in latent geometry. a** | Model $\mathbb{S}^1$ (1D sphere). The $\mathbb{S}^1$ distances d_a between pairs of nodes A_1–A_2, B_1–B_2 and C_1–C_2 (coloured in blue) are highlighted. The size of a node is proportional to its expected degree κ. **b** | Model $\mathbb{H}^2$ (2D hyperbolic disk). The same highlighted pairs of nodes (in blue) are at the same hyperbolic $\mathbb{H}^2$ distance. Higher-degree nodes are positioned closer to the centre. The angular $\mathbb{S}^1$ distances between the corresponding node pairs are the same in parts **a** and **b**. **c** | World trade map in 2013. Node colours correspond to communities detected by the critical gap method (part **e**). See Supplementary Table S1 in REF.[30] for the country associated with each acronym. **d** | Metabolic network of bacterium *Escherichia coli*. Yellow circles represent reactions and blue squares are metabolites. The name of a pathway is located at the average angular position of all the reactions belonging to it. Acronyms for metabolites are defined in the BiGG database (http://bigg.ucsd.edu/). **e** | Critical gap method. Nodes are partitioned into groups separated by void angular gaps. The modularity of the partition is computed by comparing the number of links within the communities (purple links) to the number of links between nodes in different communities (green links). The partition with the highest modularity is selected. **f** | Proximity of shortest paths in hyperbolic networks to hyperbolic geodesics. Blue arrows show the paths that geometric routing finds for two source–destination pairs in a hyperbolic network. The found paths are also the shortest paths in the network in terms of the number of hops. The hyperbolic geodesics between the corresponding sources and destinations in the hyperbolic plane are shown as dashed red curves. **g** | Structural network of the human brain with links coloured by whether they belong (magenta) or do not belong (cyan) to the minimal network that enables maximal navigability in the brain (the navigation skeleton). Parts **a,b,c** are adapted from REF.[30], CC BY 4.0 (https://creativecommons.org/licenses/by/4.0/). Part **d** adapted with permission from REF.[139], Royal Society of Chemistry. Part **g** adapted from REF.[26], Springer Nature Limited.

In this ensemble, edges are fermions with energies

$$\varepsilon_{ij} = f(x_{ij}), \tag{7}$$

where $f(x_{ij})$ can be any function of distances x_{ij} between nodes on the circle, β fixes the average energy and μ is the chemical potential controlling the expected number of edges (fermions) and thus the average degree.

The choice of $f(x)$ defines network properties in the ensemble. The necessary and sufficient conditions for networks in the model to be sparse small worlds with non-vanishing clustering are $f(x) \propto \ln x$ and $\beta \in (1, 2)$ (REF.[99]). More precisely, if $f(x) \propto \ln x$, then clustering in the $n \to \infty$ limit is zero for $\beta \leq 1$ but an increasing positive function of $\beta > 1$; networks are small worlds whenever $\beta < 2$.

The distribution of node degrees in such models is homogeneous, but the model can be modified to yield any degree distribution. Such a modification, known as the $\mathbb{S}^1$ model (FIG. 3a), sets the edge energy given in equation 7 to

$$\varepsilon_{ij} = \ln \frac{x_{ij}}{\kappa_i \kappa_j}, \tag{8}$$

and hence the connection probability in equation 6 to

$$p_{ij} = \frac{1}{1 + \chi_{ij}^{\beta}} = \frac{1}{1 + \left(\frac{x_{ij}}{\hat{\mu} \kappa_i \kappa_j}\right)^{\beta}}, \tag{9}$$

where κ_i is the expected degree of node $i = 1, \dots, n$ in the ensemble[20] and $\hat{\mu}$ is a constant that fixes the average degree. The values of parameters κ_i can be either fixed or random, sampled from any desired distribution. If they are sampled from the Pareto distribution $\rho(\kappa) = (\gamma - 1)\kappa_0^{\gamma-1}\kappa^{-\gamma}$, the resulting degree distribution is Pareto-mixed Poisson[100], which for $k \gg 1$ is a power law $P(k) \sim k^{-\gamma}$ observed in many real-world networks[101]. As in the simplest random geometric graph model, clustering is zero for $\beta \leq 1$ and an increasing positive function of $\beta > 1$. The networks in the model are ultrasmall worlds whenever $\gamma < 3$. The definition of edge energy in equation 8 combines the popularity (degrees κ_i) and similarity (distances x_{ij}) dimensions into a single measure, whereas the connection probability takes the gravity-law form in equation 9, decreasing with the similarity distance x_{ij} and increasing with the popularity product $\kappa_i \kappa_j$.

An intermediate step to go from the $\mathbb{S}^1$ to hyperbolic geometry is to map κ to y by

$$\kappa \mapsto y = \kappa^2. \tag{10}$$

This change of variables places all nodes i at coordinates (x_i, y_i), $x_i \in \mathbb{R}$, $y_i > \kappa_0^2$, in the upper half-plane model of the hyperbolic plane $\mathbb{H}^2$ (REF.[102]), which has a long history in relation to networks[88,103–108]. If $\rho(\kappa)$ is Pareto with $\gamma = 3$, then nodes are distributed uniformly on the hyperbolic plane, where the metric is $ds^2 = (dx^2 + dy^2)/y^2$. The group of distance-preserving isometries of the

half-plane is isomorphic to the Lorentz group SO(1, 2). The Lorentz boosts, which are hyperbolic rotations in the 3D Minkowski space, act on the upper half-plane as space-rescaling transformations $x \mapsto x' = \xi x$, $y \mapsto y' = \xi y$, where $\xi > 0$ (REF.[109]). The energies

$$\varepsilon_{ij} = \ln \frac{x_{ij}}{\kappa_i \kappa_j} = \ln \frac{x_{ij}}{\sqrt{y_i y_j}} \qquad (11)$$

are thus manifestly invariant with respect to rescaling Lorentz boosts, as is the model. Lorentz boosts form a non-compact subgroup of all isometries of the hyperbolic plane. However, the model is not invariant with respect to all isometries of the full Lorentz group because energy is not exactly a function of the hyperbolic distance, and hence neither is the connection probability.

This problem is fixed in a slightly different but asymptotically equivalent model, known as the $\mathbb{H}^2$ model[21], given by the map

$$\kappa \mapsto r = R - 2\ln \kappa, \qquad (12)$$

where $R = 2\ln(n/c)$ and c is the parameter controlling the average degree. This map places nodes i at polar coordinates (r_i, θ_i), $\theta_i = 2\pi x_i/n$, on the hyperbolic disk of radius R in the hyperboloid model of the hyperbolic plane with metric $ds^2 = dr^2 + \sinh^2 r \; d\theta^2$ (REF.[102]; FIG. 3b). The edge energy becomes

$$\varepsilon_{ij} = \frac{1}{2}\left(r_i + r_j + 2\ln \frac{\theta_{ij}}{2}\right) \approx \frac{1}{2}d_{ij}, \qquad (13)$$

where θ_{ij} and d_{ij} are the angular and hyperbolic distances between the two nodes. The approximation holds for a fraction of node pairs that converges to 1 in the $n \to \infty$ limit[21]. With this approximation the connection probability reads

$$p_{ij} = \frac{1}{1 + e^{\frac{\beta}{2}(d_{ij}-R)}}. \qquad (14)$$

The simplest formulation of the model is when $\rho(\kappa)$ is Pareto with exponent $\gamma = 3$ and $\beta \to \infty$: sprinkle n points uniformly at random over a hyperbolic disk of radius R, and then connect all pairs of points located at hyperbolic distance $d_{ij} < R$ from each other. The equivalence between the $\mathbb{S}^1$ model and this $\mathbb{H}^2$ representation is shown in FIG. 3b. Because energy is a function of the distance in equation 13, the model is fully Lorentz invariant in the $n \to \infty$ limit for any β.

The latent space in the model does certainly not have to be the circle $\mathbb{S}^1$. It can be any compact homogeneous space of any curvature and dimension D (REF.[99]). The higher the dimension, the lower the clustering for the same value of β (REFS[34,110]). On the hyperbolizing change of variables in equations 10 and 12, these D-dimensional spaces turn into hyperbolic spaces of dimension $D + 1$ and the edge energy becomes $\varepsilon_{ij} = \ln \frac{x_{ij}}{(\kappa_i \kappa_j)^{1/D}} \approx d_{ij}/2$ (REF.[99]).

The models have been also adapted to growing networks[35] — in which case the latent space is not hyperbolic but de Sitter space $d\mathbb{S}^{1,D}$ with the same Lorentz group $SO(1, D+1)$ of symmetries[111] — and to weighted networks[112], multilayer networks[113,114] and to networks with community structure[29,32,115]. The model has yet to be extended to directed networks, because it is not clear how to reconcile the intrinsic symmetry of metric distances with asymmetric interactions among nodes.

The equivalence between the two models in equations 8 and 13 is a reflection of the isomorphism between the Lorentz group $SO(1, D+1)$ and the Möbius group acting on sphere $\mathbb{S}^D$ as the group of its conformal transformations. This isomorphism is a starting point of the anti-de Sitter/conformal field theory correspondence in string theory[116].

It is important to re-emphasize that the latent space in the described models can indeed be any compact homogeneous space of any dimension D (REF.[99]). This space can also be flat, or positively or negatively curved. However, the effective space of the higher dimension $D + 1$ is always hyperbolic, that is, negatively curved. What makes this space hyperbolic is the simple change of variables in equations 10 and 12, which maps the expected degrees of all nodes to their $D + 1$th (radial) coordinates. On this change of variables, the probability of connections is always a function of hyperbolic $D + 1$-dimensional distances only (equations 13 and 14). However, the nodes are distributed uniformly according to the metric in this $D + 1$-dimensional hyperbolic space only if the degree distribution is a power law with exponent $\gamma = 3$, that is, only if $\rho(\kappa)$ is Pareto with $\gamma = 3$.

Another important observation is that, as was shown recently in REF.[99], the described models are unique latent-space network models that satisfy certain maximum-entropy requirements and that produce sparse heterogeneous uncorrelated small worlds with non-zero clustering. At present, these models are also the only known class of network models that capture all the following properties of many real-world networks: sparsity, self-similarity, small-worldness, heterogeneity, non-vanishing clustering and community structure. As a result, this ensemble of random graphs has attracted substantial research attention in mathematics and theoretical computer science, fields in which many basic and advanced properties of random hyperbolic graphs have been (re)derived rigorously[117–128].

Hyperbolic maps of real-world networks. A collection of methods have been developed to infer the coordinates of the nodes of a real-world network in its latent space.

Many generative-model-based methods perform statistical inference using Monte Carlo sampling and maximum likelihood estimation[97,129–131]. Data-driven methods vary in flavour. One such method is unsupervised machine learning, which is used, as in coalescent embedding[132], to implement nonlinear dimension reduction[133]. Other data-driven methods rely on the network community structure[31,134]. Mechanistic-model-based methods map the network while unfolding the similarity space[135]. Generative models and data-driven models both have advantages and disadvantages in terms of accuracy and speed, so hybrid models have been developed[136,137]. Hybrid methods obtain initial coordinate estimates using machine learning techniques, and then refine the results via maximum likelihood

estimation. In general, the main challenge that hyperbolic network mapping methods face is the abundance of local maxima in highly non-convex likelihood landscapes. An efficient way to escape from these maxima — thus boosting the inference accuracy — is to shake the system by adding decreasing levels of noise to it[138], a method conceptually similar to simulated annealing.

The application of these methods to real-world networks makes it possible investigate them at different resolutions using the latent-space RG, which unfolds the network in a sequence of self-similar layers, or renormalization shells[34]. The maps of real networks[30,139] (FIG. 3c,d) also revealed the existence of geometric communities and helped decode mechanisms that govern network evolution, such as globalization, localization and hierarchization, which drive the evolution of international trade[30]. Such maps have also shed light on many dynamical processes in real-world networks, showing, for instance, that cooperation in social networks is controlled more strongly by the latent-space organization than by highly connected hubs in the system[140]. Another class of applications of hyperbolic maps of real networks is link prediction. Because the connection probability in the described models is a decreasing function of the latent hyperbolic distance, the models predict that links are more likely to exist between hyperbolically closer pairs of nodes. Link prediction using hyperbolic geometry has been analysed from different angles[135,138,141,142]. It appears to be particularly powerful when it comes to predicting links that are difficult to predict, such as links between nodes without common neighbours[138]. Finally, one of the most practical applications of mapping real-world networks to their latent geometries is the design of efficient routing protocols for the Internet[97] and for emerging Internet-of-Things telecommunication networks[143]. We discuss some of these applications below.

Geometric communities. In the above models, the angular distribution of nodes is uniform. However, nodes in maps of real networks are clustered in regions that define geometric communities. Such communities have been observed in many real networks, including the Internet[97], metabolic networks in cells[139], trade networks[30] and brain connectomes[144]. Non-overlapping communities can be detected in the geometric domain using purely geometric methods. One definition considers soft communities as groups of nodes in similarity space separated from the rest by angular gaps that exceed a certain critical value[139]. An alternative, known as the critical gap method[30], finds the communities by changing the gap and selecting the soft community partition that maximizes the standard modularity measure (FIG. 3e). These distance-based communities show strong correlations with groups defined by metadata, such as geographical location of the autonomous systems in the case of the Internet[97], biochemical pathways of reactions in metabolic networks[139] or anatomical brain regions in structural brain networks[27,145]. Geometry-based communities also overlap substantially with topology-based communities, making the geometric nature of complex networks even more evident[30,146].

Geometric communities affect degree–degree correlations and the functional form of the clustering spectrum in the network ensemble. In the 'vanilla' version of the model described above with the homogeneous distribution of angular coordinates, these properties are not tunable but are fixed by structural constraints[147,148]. However, if these coordinates are not homogeneously random but instead set by their heterogeneous values inferred in a real network with communities, the ensemble of random networks generated by the model using these heterogeneous inferred coordinates accurately reproduces the degree correlations and clustering in the real network[137,138]. This observation suggests that, to a great extent, degree correlations are a consequence of latent geometry coupled with inhomogeneous distributions of nodes in it.

Navigability. Latent space guides navigation in the network based on distances between nodes in the space[25]. That is, instead of finding shortest paths in the network — a computationally intensive combinatorial problem in a network that changes dynamically, such as the Internet[149] — a transport process can be geometric, relying only on geodesic distances in the space. The efficiency and robustness of such processes[28] determines how navigable a network is. Navigability is improved for smaller γ and larger β, thereby defining a navigable parameter range to which many real-world networks belong[25]. Networks in the hyperbolic model described above are nearly maximally efficient for such geometric navigation[21], which has recently been proven rigorously[121].

The main reason behind this phenomenon is the existence of shortest paths close to the corresponding geodesics in the underlying hyperbolic geometry (FIG. 3f) for any pair of nodes in hyperbolic networks. Another critical factor is the existence of superhubs that interconnect all parts of the network, present as soon as $\gamma < 3$ (REF.[21]), in which case the networks are known as ultrasmall worlds[52]. Navigation in hyperbolic networks with $\gamma < 3$ can always find these ultrashort paths[96]; thus, navigation in these networks is asymptotically optimal. Conversely, networks that are maximally navigable by design are similar to hyperbolic networks[26], and many real-world networks, such as the human brain (FIG. 3g), contain large fractions of their maximum-navigability skeletons[26]. Assuming that real-world networks evolve to have a structure that is efficient for their functions, these findings provide an evolutionary perspective on the emergence of the latent geometry that leads to structural commonalities observed in many different real-world networks.

Renormalization and self-similarity. Networks in the discussed models are purely scale invariant in the thermodynamic limit, and thus contain an infinite hierarchy of self-similar nested subgraphs induced by nodes that have degree exceeding a given threshold (BOX 1). This observation applies to many real networks, for which the average degree of the subgraphs increases as a function of the degree threshold[150]. This property makes it possible to prove the absence of percolation or epidemic thresholds in such networks[150], independently of the commonly used tree-like or scale-free assumptions[151].

The proof is general and is based solely on a symmetry principle. Thus, it also applies to any phase transition for which the critical point is a monotonic function of the average degree[150]. Examples of models for which the proof holds include susceptible–infected–susceptible (SIS)-type epidemic spreading, which in scale-free networks lack a healthy phase[152] or the Ising model, which in scale-free networks lacks a disordered phase[153–155].

Self-similarity is also observed in the multiscale organization of networks, and can be explored at different resolutions by applying a geometric renormalization transformation[34] inspired by concepts from the real-space RG in statistical physics[58,59,156]. The method takes a different approach to that of the shortest-path-distance RG discussed above, as it relies on distances in the similarity subspace to coarse-grain neighbouring nodes into supernodes that define a new rescaled map (BOX 1). The iteration of the transformation unfolds a network into a multiscale shell that progressively selects longer-range connections, revealing the co-existing scales and their interactions. Self-similarity under geometric renormalization is a ubiquitous symmetry in real-world networks (FIG. 4a–c), in good agreement with the prediction given by the renormalizability of the underlying $\mathbb{S}^1$ model[34] (FIG. 4d–f). This result suggests that the same connectivity law rules short- and long-range connections, and operates at different length scales. Interestingly, the structure of the human brain remains self-similar when the resolution length is progressively decreased by hierarchical coarse-graining of the anatomical regions, a symmetry that is predicted by geometric renormalization[144]. From a practical point of view, applications of self-similarity under geometric renormalization include a multiscale navigation protocol that takes advantage of the increased navigation efficiency at higher scales, and scaled-down network replicas. In these network replicas, the behaviour of dynamical processes — such as SIS epidemic spreading, the Ising model or the Kuramoto model[157] — is preserved across layers (FIG. 4g–i).

Open questions. In neuroscience, geometric navigation as discussed above offers a possible explanation and mechanism for the routing of information in the brain. This hypothesis has been investigated at different depths and from different perspectives[158–167]. Geometric navigation is effective only when the network topology is congruent with the underlying latent geometry so that following geodesic paths in the latent space is equivalent to navigating through topological shortest paths. This equivalence seems to hold for structural brain networks whose many structural and navigability properties are well described by the $\mathbb{S}^1/\mathbb{H}^2$ geometric network model[27,145], for which the same connectivity laws apply both to short-range and long-range connections and at different scales[144]. Thus, simplicity might be one of the main organizing principles of human structural brain networks — at least at the macroscale level, which displays a self-similar architecture across different anatomical length scales, in good agreement with the discussed geometric models[144], unlike traditional approaches that describe brain connectivity using Euclidean

geometry[168–170]. Euclidean distances certainly do play a role in the brain. However, they are not the only factor determining similarity, and thus connectivity, between brain regions[27,144]. More recently, data-driven dimensional reduction techniques[145,171] and local curvature measures[172] have been proposed as alternative geometric descriptions that avoid the definition of connectivity laws. It remains unknown how the hyperbolic geometry of the brain relates to the widely accepted optimization principles that Santiago Ramón y Cajal hypothesized more than a century ago as the two forces ruling the evolution of mammalian brain connectivity: minimizing wiring costs and maximizing conductivity speed[173].

In the context of machine learning, primarily after the publication of REF.[174], hyperbolic spaces have ignited vigorous research activity. This activity has been applied to many settings and tasks including embedding graphs and other data, such as images and texts, as well as in the design of neural networks, attention networks and knowledge graphs, with applications including data classification, image recognition, natural language processing, link prediction and scalable recommender systems[175–185]. Overall, the main flavour of these results confirms one of the main points in REF.[21]: compared with Euclidean geometry, hyperbolic geometry appears to be a better (embedding space) model for highly heterogeneous networks and other data.

In terms of open questions, perhaps one of the most common ones is how to tell whether a given (real world) network has a latent (hyperbolic) space. This question is a variant of the more general question of how to tell whether a given model is a good model for a given network. Such questions can never find positive answers because one can never learn a model or a distribution based on one sample from it. Neither can one know for sure whether any given network has typical values of all possible network properties in any given model, simply because the number of such properties is infinite[186]. One can always check if any finite collection of properties of the network have the typical values in the model, and as soon as an atypical property is found, one may raise doubts how good the model is for the network at hand. Such a finding does not always render the model useless. For instance, clustering is zero in stochastic block models and non-zero in real-world networks, but this fundamental mismatch does not appear to diminish much the interest in stochastic block models, owing to their simplicity and tractability.

The latent-space models described above reproduce most of the important properties of real-world networks. What this means is that any network that has these properties can be mapped to a latent space of any dimension, yielding some non-trivial results. What space dimension one should choose for the embedding[132,187] is an interesting open problem. Solving it requires identifying a network property that would depend on the space dimension in a known way. At present, it is known that clustering is a decreasing function of dimension[34,110], but it is also a decreasing function of temperature[20,21], so that the value of clustering by itself cannot tell us the likely value of the space dimension. In the absence of such understanding, and
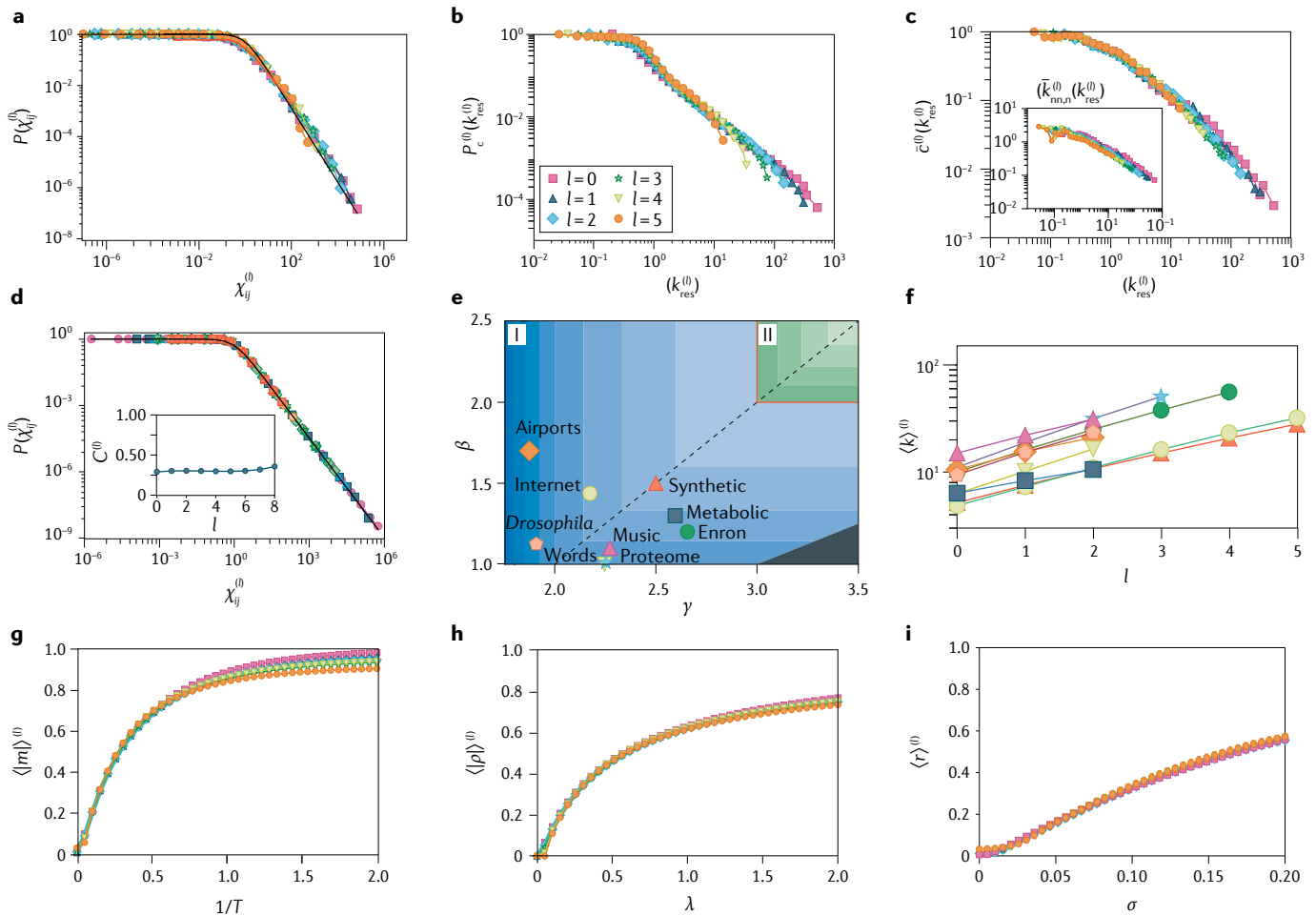
Fig. 4 | **Multiscale unfolding of network structure and function by geometric renormalization. a–c** | Self-similarity of the structural and dynamical properties of the multiscale five-layered geometric renormalization shell of the Internet, in terms of the empirical connection probability in layer l of renormalization, measured as the fraction of connected pairs of nodes (denoted i and j) as a function of the rescaled distance $\chi_{ij}^{(l)}$ as defined in equation 9 (part **a**); complementary cumulative distribution $P_c^{(l)}$ of rescaled degree $k_{res}^{(l)}$ (part **b**); and degree-dependent clustering coefficient $\bar{c}^{(l)}$ over rescaled-degree classes (part **c**; inset shows normalized average nearest-neighbour degree $\bar{k}_{nn,n}^{(l)}$). **d** | The same as in part **a**, but for a synthetic $\mathbb{S}^1$ network with $N \approx 225{,}000$ nodes, scale-free exponent $\gamma = 2.5$ and inverse temperature $\beta = 1.5$. The black dashed line shows the theoretical curve given in equation 9. Inset: invariance of the mean local clustering $C^{(l)}$ along the flow. **e** | Real networks in the connectivity phase diagram of the $\mathbb{S}^1$ renormalization flow. The synthetic network of part **d** is

also shown. Darker blue (green) in the shaded areas represent higher values of the exponent c controlling the flow for the average degree $\langle k \rangle^{(l+1)} = r^c \langle k \rangle^{(l)}$. The dashed line separates the γ-dominated region from the β-dominated region. In phase I, $c > 0$ and the network flows towards a fully connected graph. In phase II, $c < 0$ and the network flows towards a 1D ring. The red line $c = 0$ indicates the transition between the small-world and non-small-world phases. In region III, the degree distribution loses its scale-freeness along the flow. **f** | Exponential increase of the average degree of the renormalized real networks $\langle k \rangle^{(l)}$ with respect to l. **g–i** | Simulation of the Ising (part **g**), susceptible–infected–susceptible (SIS) (part **h**) and Kuramoto (part **i**) models in scaled-down replicas of the real Internet. The dynamics is preserved even in small replicas 2^5 times smaller than the original network. m, magnetization; T, temperature; ρ, prevalence; λ, infection rate; r, coherence; σ, coupling strength. Results in parts **g–i** are averaged over 100 simulations. Parts reprinted from REF.[34], Springer Nature Limited.

given that space in hyperbolic geometry expands exponentially fast in any dimension, which minimizes any distortions of low-dimensional mappings, there are no reasons not to choose the simplest case $D = 1$ for the embedding, unless overparametrization may be beneficial, as in deep learning[188].

Another important open problem is to identify a collection of network properties that are not only necessary but also sufficient conditions for latent geometricity. This problem is not about any given network, in which case it can never be solved for the reasons given above, but about network models. For instance, the question about whether clustering is such a property

can be formulated as follows: is a model that reproduces clustering but produces otherwise maximally random networks equivalent to a latent-space model? Such questions cannot be answered without additional stringent assumptions and requirements, such as the requirement of maximum entropy. The first steps in this directions have been made in REFS[99,189].

Other open problems, which are interesting from the practical perspective, are to study the coupling of dynamical processes with the latent space and to generalize latent-space network models to temporal networks[190]. It has been observed that clusters in the underlying metric space emerge in evolutionary games

on scale-free networks[140]. Other processes could present geometric patterns in their dynamical states as well. A key point is that essentially all real-world networks are highly dynamic at different timescales, suggesting that the positions of nodes in the latent space cannot be fixed but must constantly change. However, the development of dynamic latent-space models is challenging, because there is no consensus or even general understanding concerning the exact set of requirements for such models. The main high-level problem is that there are too many 'degrees of freedom' in designing these models, that is, arbitrary choices can be made, and there are no generally agreed guiding principles concerning what choice is better or worse.

At a more fundamental level, the fact that hyperbolic networks are Lorentz invariant in the thermodynamic limit suggests the need to re-examine the role of probabilistic symmetries[191] in the theory of graph limits[192]. Traditionally, the main symmetry of interest in that context has been exchangeability[193] — the requirement that the probability of a graph in an ensemble does not depend on how nodes in the graph are labelled, reminiscent of gauge invariance in physics. This requirement is stringent for deep statistical reasons[193], but it is also easy to appreciate intuitively: if node labels $1, \ldots, n$ are just random 'coordinates' used to represent an otherwise unlabelled graph as an adjacency matrix, then the probability of the graph in the ensemble cannot depend on these meaningless coordinates. However, the Aldous–Hoover theorem[194,195] states that graphs in the thermodynamic limit of any exchangeable graph ensemble are either dense or empty. This fact is in an unsettling disconnect with real-world networks, a vast majority of which are sparse. Therefore, different notions of exchangeability-like probabilistic symmetries have been investigated for sparse graph limits[196–199]. Because of the Aldous–Hoover theorem, they all depart from the $1, \ldots, n$ 'coordinate system' for node labels, and rely on different systems of node or edge labels. The Lorentz invariance of hyperbolic networks suggests that the labels of nodes can be indeed their coordinates in a latent space, with exchangeability replaced by invariance with respect to the space isometries. The hope is that such ensembles may have some interesting and tractable thermodynamic limits.

Dynamic geometry of network processes

The existence of a hidden geometry of network structure naturally raised the question of whether a hidden geometry of network dynamics was plausible. The motivation for this question is to identify the latent space due to system function that arises from the interplay between structure and dynamics. Note that network dynamics is broadly defined, and includes the dynamics of vertex and edge creation or destruction — exemplified by network growth processes or time-varying topologies[190], for example — and the dynamics of processes on the network. The hidden geometry induced by dynamics has been mostly explored for the latter, except for a few notable cases[200].

Geometric tools have proved fruitful for unravelling hidden patterns lurking in the complex behaviours of network-driven processes. From the spread of rumours and opinions in sociotechnical systems to the global spread of innovations and epidemics, combining dynamics with the self-similar structure of complex networks and their latent geometry results in heterogeneous processes that cannot be easily understood when investigated in the Euclidean space where they are often embedded. However, when the same dynamical processes are analysed through the lens of the geometries they induce, one often discovers simple and elegant arguments to better understand the complex spatiotemporal patterns observed in a broad spectrum of complex systems.

Because it is possible to define multiple dynamical processes on the network — such as epidemic spreading (FIG. 5) or random searches (FIG. 6) — one does not expect to find a unique latent geometry for the system's functioning: in principle, there could be as many hidden geometries as the number of plausible network-driven processes.

In this universe of dynamical processes, the dynamics of information exchange has mostly been modelled through diffusive processes, for which the amount of matter being diffused is conserved, and spreading processes, in which the amount of matter being diffused is duplicated at each step (as in the spreading of viruses or ideas) and consequently is not conserved. Such dynamics have been successfully exploited to define metric or quasi-metric measures to probe the corresponding latent geometry. The difference between metric and quasi-metric measures is that, in the latter, the symmetry axiom is relaxed.

Remarkably, these classes of network geometry, induced by kinematic distances, provide results about a system's function that cannot be obtained by geometric approaches discussed in the previous sections. An emblematic example concerns the mesoscale organization of interconnected components that exchange information during collective phenomena — such as coupled oscillators trying to synchronize or people with social relationships attempting to reach consensus — which can be characterized by mapping the interplay between structure and function to a geometric space induced by diffusion dynamics[42]. The resulting functional modules differ from the ones obtained by other geometric techniques such as functional modularity maximization[65], because the latter finds an optimal partition of the system while minimizing the possible number of modules of given topological size ℓ, which in turns defines the characteristic distance between nodes within modules. Conversely, modules identified on the diffusion manifold at time τ, determining the scale of dynamics, are characterized by groups of nodes that easily exchange information — for instance, in terms of random searches — within Markov time τ, as we discuss here.

Geometry induced by resistance. In first approximation, one can model information exchange in a network with a model similar to that of current flow in a circuit. This approach is probably among the first historical attempts to quantify a distance between nodes in terms of a (simple) dynamics. This resistance distance R_{pq} (REF.[201])
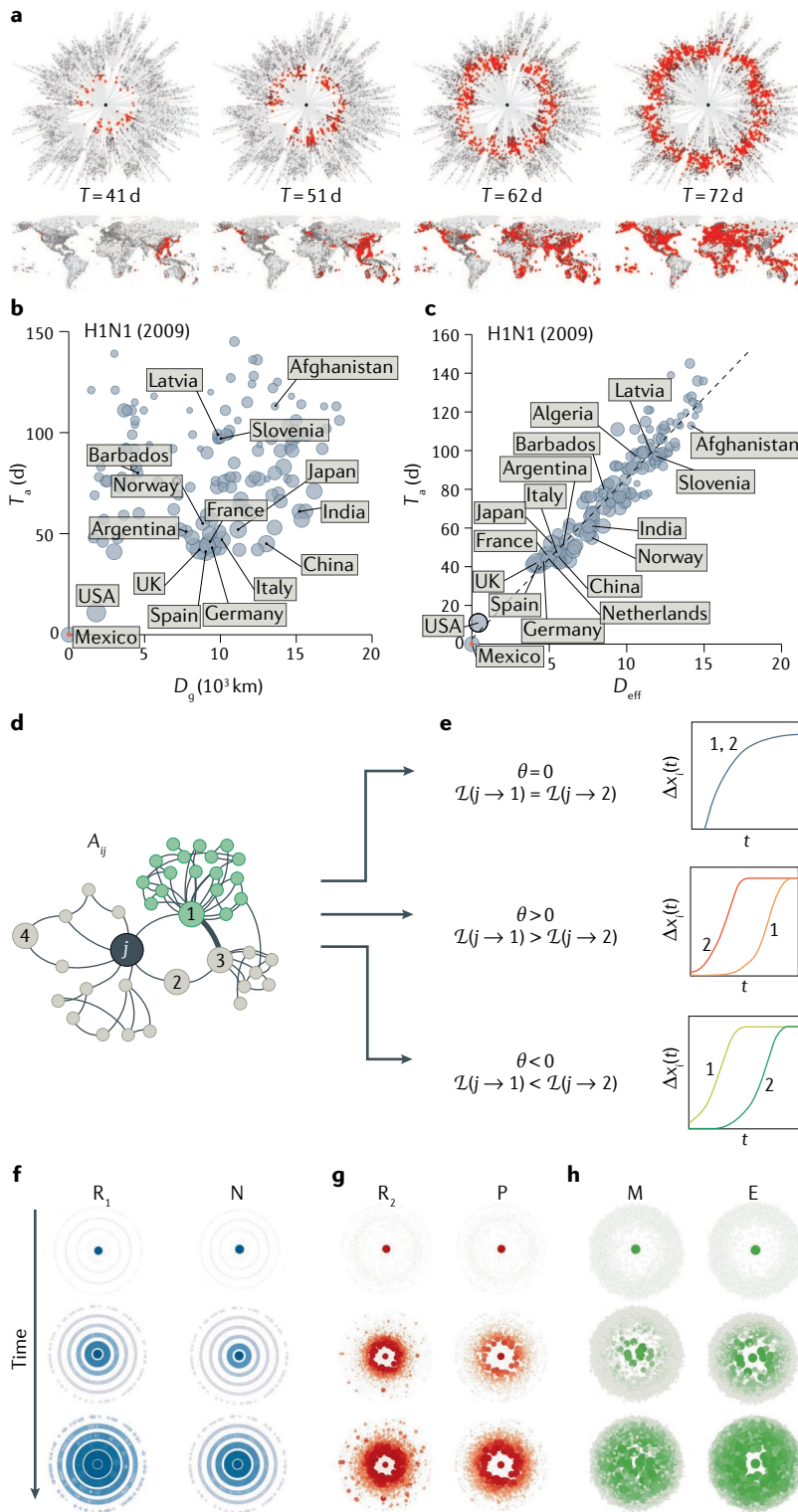
Fig. 5 | Geometry induced by spreading dynamics and universal temporal distance. a | Evolution of a simulated disease spreading originating in Hong Kong: red symbols encode the prevalence. Top panels show the evolution in the latent space; bottom panels show the same dynamics in the natural space. When the spreading dynamics is depicted by exploiting the induced geometry, complex spatial patterns are mapped to homogeneous wave fronts propagating at constant effective speed. **b,c |** Relationship between epidemic arrival times (T_a) and the two distances for the spreading of influenza A virus subtype H1N1. The relation is nonlinear when geographic distance D_g is used (part **b**) whereas it is nicely reproduced by a straight line when effective distance D_{eff} is considered (part **c**). **d,e |** A signal travelling from vertex j to the rest of the system exhibits different spreading patterns (part **d**), captured by the universal temporal distance $\mathcal{L}(j \rightarrow i)$, impacting different nodes (such as nodes 1 and 2) in different ways (part **e**) depending on the type of dynamics, described by the parameter θ: distance limited ($\theta = 0$; top); degree limited ($\theta > 0$; middle); or composite ($\theta < 0$; bottom) A_{ij} indicates the corresponding entries of the adjacency matrix; $x_i(t)$ indicates the ith entry of the state vector at time t. **f–h |** The homogeneous propagation of concentric wave fronts emerge from the analysis of a broad spectrum of synthetic and empirical systems. R_1 and R_2 indicate models capturing regulatory dynamics, M captures ecological interactions, E captures epidemic spreading, N captures neuronal activation and P captures population dynamics. Parts **a–c** adapted with permission from REF.[40], AAAS. Parts **d–h** adapted from REF.[43], Springer Nature Limited.

where $\Omega = \mathbb{L}^\dagger + N^{-1}\mathbb{U}$, and N is the size of the network, $\mathbb{U}$ is a matrix with all entries equal to 1 and $\mathbb{L}^\dagger$ is the Moore–Penrose inverse of the Laplacian matrix of the network. On the one hand, this metric has been successfully used, for instance, to analyse specific isomers[202] and genetic differentiation[203]. On the other hand, it has been also shown that, for some classes of graphs, the resistance distance converges to the trivial thermodynamic limit $k_p^{-1} + k_q^{-1}$, where k indicates the node degree[204], reducing the usefulness of this metric for the analysis of most empirical systems.

Geometry induced by communicability. One of the first metrics based on dynamics was the communicability distance[87,205]. This metric can be introduced by starting from the concept of communicability between two nodes i and j of a network, which is defined as $G_{ij} = \exp(A)_{ij}$, where A is the underlying adjacency matrix. From a mathematical point of view, communicability quantifies how well a pair of nodes exchanges information by all possible walks between them, giving more weight to the shortest ones, as can be understood by considering the Taylor expansion of the communicability matrix G (REFS[87,205]).

Communicability can also be understood from a physical perspective. Consider a network where nodes are harmonic oscillators and links are springs, and the system is submerged into a thermal bath with inverse temperature $\beta = 1/k_B T$, where k_B is the Boltzmann constant. Then communicability provides a representation for the thermal Green's function of the system, indicating

between two nodes p and q of a network is calculated by assuming fixed resistors on each network edge: the corresponding circuit — under the further assumption that p and q are directly connected by a battery to allow electric currents to flow — allows for the calculation of effective resistances as

$$R_{pq} = \Omega_{pp} + \Omega_{qq} - \Omega_{pq} - \Omega_{qp}, \tag{15}$$

a Original network **b** Induced geometry **c** **d** **e** Rhesus macaque
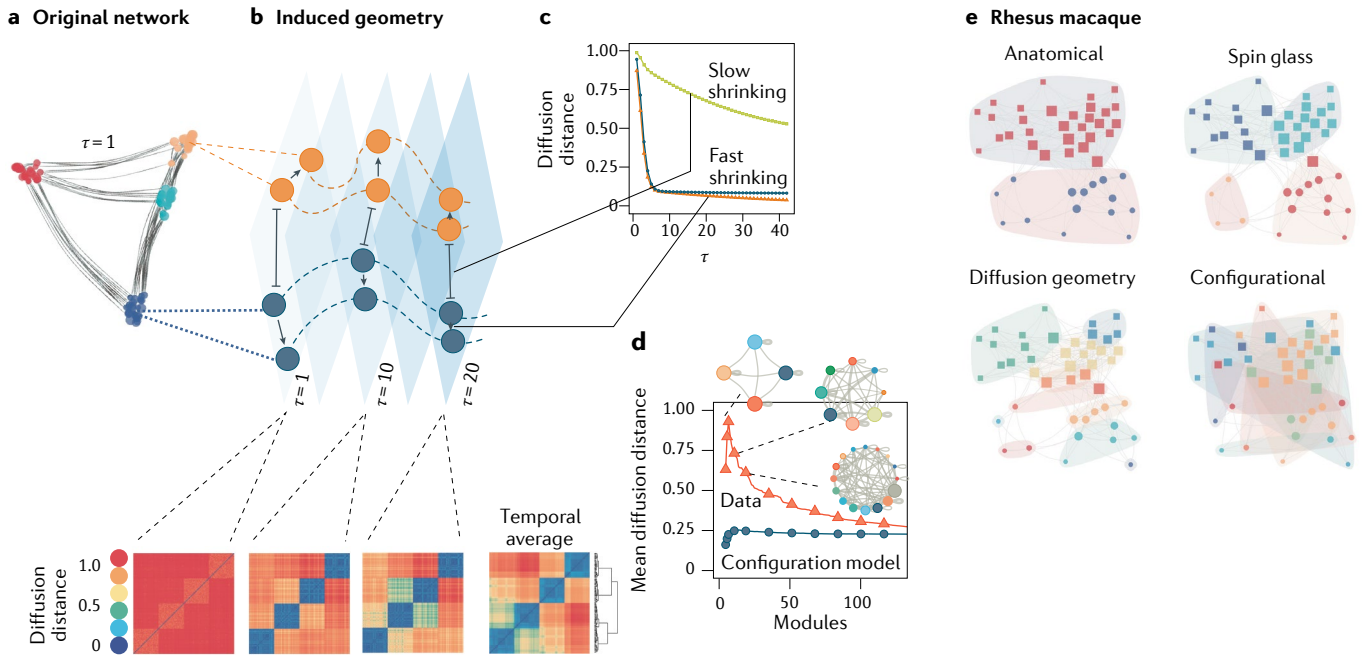
Fig. 6 | **Diffusion geometry of complex networks and multilayer networks. a** | Euclidean embedding of a network with four clusters. The embedding provides a representation of the latent diffusion geometry with Markov time $\tau = 1$. **b,c** | In the diffusion space, two nodes from the same functional cluster are (and remain) closer across time, τ, than nodes belonging to different clusters. Diffusion-distance matrices corresponding to different times are shown at the bottom and allow identification of the underlying functional organization at different scales. **d** | The functional modules that maximize the average diffusion distance define the mesoscale structure that favours the overall information exchange. The significance of this structure can be quantified by comparing against the result obtained from a configuration model preserving the degree distribution of the original data while destroying other correlations. **e** | Diffusion geometry analysis of the anatomical connectivity (335 visual, 85 sensorimotor and 43 heteromodal) from 30 visual cortical areas and 15 sensorimotor areas in the macaque monkey. Clusters identified by structural analysis of the connectome using the spin-glass approach are different, as the anatomical organization and the mesoscale organization obtained from the configuration model. Figure adapted with permission from REF.[42], American Physical Society.

how a thermal oscillation propagates between nodes. The difference between the absorbed and transmitted excitation between two nodes due to such thermal disturbances is quantified by the communicability distance[205]

$$\xi_{pq}(\beta) = G_{pp}(\beta) + G_{qq}(\beta) - 2G_{pq}(\beta), \qquad (16)$$

which enables building a hyperspherical embedding of a complex network[206] at different temperatures. This graphical embedding yields a representation of a geometry that is able to capture, for instance, spatial efficiency of networks[207], traffic flows in cities[208] and constrained diffusion in coupled networks[209] such as multilayer systems[210]. Because the topic is vast and beyond the scope of the present Review Article, we refer the interested reader to REF.[211] for a thorough review of the mathematical and physical properties of communicability distances in complex networks. We also stress that, as well as the communicability distance, other important generalizations of the traditional shortest-path distance have been investigated in mathematics[212,213].

Geometry induced by reaction–diffusion. Another important class of geometry that is induced by network dynamics is obtained by considering a quasi-metric

as effective distance, and can be used to gain insights about reaction–diffusion processes such as the spreading of infectious diseases through mobility networks[40,214]. Given a network of geographic areas (such as airports) and edges encoding direct air traffic (in units of passengers per day) from node i to node j, let F_{ji} indicate the corresponding mobility flow. The connectivity matrix P, with components $P_{ij} = F_{ij}/\Sigma_i F_{ij}$, quantifies the fraction of this flow originating from node j directed towards node i. Despite the structural complexity of the network, involving multiple and often redundant pathways for the transmission of contagion phenomena, the effective distance defined by

$$\delta_{ij} = 1 - \log P_{ij}, \qquad (17)$$

reveals hidden geometric patterns in which the dynamics of epidemic spreading is elegantly mapped into the propagation of wave fronts with an effective speed. This latent dynamic geometry can be used to better predict the arrival times of empirical contagion processes in distinct geographic areas and to reconstruct, with reasonable accuracy, the origin of outbreaks (FIG. 5a–c).

Similarly, the collective dynamics of spatiotemporal propagation of signals on networks can be interpreted by looking at the effect of the geometry induced by their

dynamics on the definition of the universal temporal distance[43]

$$\mathcal{L}(j \rightarrow i) = \min_{\Pi(j \rightarrow i)} \left\{ \sum_{p \in \Pi(j \rightarrow i), p \neq j} S_p^{\theta} \right\}. \tag{18}$$

In equation 18, $\Pi(j \rightarrow i) = j \rightarrow q \rightarrow \ldots \rightarrow i$ indicates the shortest path from node j to node i. The delay τ_p in signal propagation occurring on each node $p \in \Pi(j \rightarrow i)$ is assumed to scale as $\tau_p \sim S_p^{\theta}$, where $S_i = \Sigma_k A_{ik}$ is the weighted degree of node i and $\theta = -2 - \Gamma(0)$, and where Γ is a parameter determined by the system's dynamics. This metric yields excellent predictions about the actual propagation times $T(j \rightarrow i)$ for a range of non-linear dynamic models (FIG. 5d,e). Furthermore, despite their diversity, disparate propagation patterns actually condense into three distinct dynamic regimes (FIG. 5f–h) characterized by the interplay between network paths, degree distribution and the interaction dynamics[43].

In the same spirit, spreading processes on noisy geometric networks[215,216] have been recently investigated to understand how contagion dynamics is driven by the underlying topology[41]. Noisy geometric networks provide a suitable framework to model systems characterized by both short-range (that is, large world) and long-range (that is, small world) interactions among nodes. Contagion maps, which have a manifold structure that reflects the interplay between local structure, non-local structure and the epidemic spreading process, provide a suitable tool to recover the geometric features of a network's underlying manifold and describe wave front propagation in the corresponding geometric space. This geometric framework yields physical insights on contagions by exploiting computational topology and allows identification of low-dimensional structure in complex networks[41].

Geometry induced by random search. More recently, random walk dynamics has been proposed to define a diffusion distance between pair of nodes. For a random walk that starts in node i with probability 1, the evolution over time τ of the probability to find the walker in any node is described by a master equation[81], the solution of which is given by $\mathbf{p}(\tau|i) = \mathbf{e}_i \exp(-\tau \mathcal{L})$, where $\mathbf{e}_i \equiv (0, 0, \ldots, 1, \ldots, 0)$ is the ith canonical vector in the Euclidean space with dimension N, the size of the system, and $\mathcal{L} = I - T$ is the normalized Laplacian matrix, with I_{ij} the Kronecker delta and T_{ij} the probability for the random walker to move from node i to node j. The hidden geometric space induced by the random walker's Markov dynamics[42] is characterized by the diffusion distance between nodes i and j, defined by

$$d_{i,j}(\tau) = ||\mathbf{p}(\tau|i) - \mathbf{p}(\tau|j)||, \tag{19}$$

which provides the starting point to build diffusion maps which are widely adopted for low-dimensional embedding of high-dimensional data[39], among other applications. Two nodes are close in their latent diffusion space if they are connected by multiple pathways that facilitate information exchange in less than τ steps.

As a direct consequence, the mesoscale functional organization of the network is mapped into spatial clusters in the corresponding diffusion manifold, with Markov time playing the role of a multiresolution parameter, that is, a temporal length scale playing the dynamic analogue of the shortest-path distance or the similarity metrics used in latent spaces.

This latent diffusion space has many applications. Studying it at increasing values of τ allows identification of functional hierarchies at multiple temporal resolutions, the persistence of which across time identifies the mesoscale structure that favours the overall information exchange, providing the best coarse-graining of the system in functional modules (FIG. 6a–e). Microscale, mesoscale and large-scale structures can be probed for small, increasing and large τ, respectively. Geometry induced by diffusive processes reveals physical insights about collective phenomena in structured populations, by establishing a formal relationship with complex dynamics responsible for synchronization in the metastable state and emergence of consensus. The recent application to anatomical connectivity within and between visual cortical and sensorimotor areas in macaque brain reveals a hierarchical functional organization of cortical units, not identified by existing methods and not compatible with null models[42] (FIG. 6e). The network embedding in a geometric space induced by diffusion distance, together with statistical data depth, allows for the statistical and most natural generalization of the concept of median to the realm of complex networks. This generalization has advantages for defining the centre of the system and percentiles around that centre to identify vertices that are socially or biologically relevant[217].

More recently, it has been proposed to extend the framework to the realm of multilayer networks[218], capitalizing on the generalization of different random walk dynamics to multilayer systems[210,219,220]. In fact, layer–layer topological correlations might alter information exchange among state nodes, and the presence of different interlayer connectivity patterns might lead to distinct geometric regimes. It appears that when the fraction of interlinks is small, flow is segregated within layers and the diffusion manifold consists of two well-separated submanifolds, corresponding to the functional organization of each layer separately, connected by weak geometric pathways; when the fraction is sufficiently high, the flow is integrated, new geometric pathways are made available for information to be exchanged across layers and those submanifolds mix up. Different multilayer diffusion manifolds have been used to better understand the functional organization of multimodal transportation and multiplex social systems[218].

Open questions. The results discussed above make the geometry induced by network-driven processes perhaps the most suitable framework for several practical applications, such as predicting the time course of dynamics for forecasting and control of spreading processes, and locating their origin. Indeed, diffusion geometry defines a class of models that have the desirable advantages of being mathematically tractable and readily interpretable.

The research programme for the future is broad, with open challenges of both theoretical and practical relevance. On the one hand, the topological organization of empirical complex systems can be characterized in terms of hierarchies[221,222] and mesoscale structures such as bow-tie[223,224], k-cores[225,226] and core–periphery[227,228]; thus it will be interesting to identify and characterize their functional counterparts in terms of diffusion geometry. The main challenge is to define mesoscale objects such as functional giant components and functional cores. On the other hand, research is needed to better understand the deep relationships among the aspects of network geometry discussed in this Review Article. A promising step towards building a theoretical bridge is provided by the concept of communicability, which can be understood in purely combinatorial terms as an effective pathway — weighting in a specific way the contributions of walks of different lengths — between nodes in the network space. In this regard, it is intimately related to the concept of geometrical navigability, for instance, which is determined by selecting topological paths that follow geodesics in the latent space. In general, those paths happen to be topological shortest paths when networks are sufficiently congruent with the latent space. Note that congruency can be defined in different ways, not only in terms of greedy shortest paths[21,27,97,229] but also by taking into account all topological shortest paths[230].

As for further open challenges, developing RG techniques in the space induced by diffusion distances is a fundamental open problem, the solution of which could shed light on the self-similar symmetries of dynamical processes evolving on top of complex networks. Such techniques could further pave the way to the analysis of co-existing temporal scales due to the interplay between structure and dynamics. Finally, a natural development of geometries induced by network-driven processes is the identification and characterization of a more general framework in which diffusive dynamics are replaced by more complex ones. This advance would improve our understanding of complex dynamical processes and has the potential to enhance the control and forecasting of the evolution of empirical systems.

Other flavours of network geometry
Network geometry comes in flavours other than those discussed in detail in this Review Article. Here, we discuss advances and open challenges in some of those areas.

Geometrogenesis. Perhaps one of the most fundamental open problems in network geometry is that of geometrogenesis, that is, the emergence of continuous geometric spaces from discrete combinatorial rules. The study of emergent geometries has gained momentum[231,232] from its intimate connections with long-standing combinatoric problems in several approaches to quantum gravity, such as causal sets[233,234], quantum graphity[235] and causal dynamical triangulations[236]. In loop quantum gravity, for example, the basis of states is formed by spin networks that have support on a graph, determining a sort of quantum geometry in which the intrinsic geometry — consisting

of quanta of space — is discrete and the extrinsic curvature is fuzzy because of Heisenberg's uncertainty principle[237]. The main challenge is to assign a classical geometrical interpretation to such states. Advances have been made in this direction based on operators that quantize both scalar and mean curvature when spin network edges run within the surfaces of the quantized geometry[238]. In quantum graphity[235], the space is a dynamical graph that evolves under the action of a Hamiltonian. In causal dynamical triangulation[239], a non-perturbative path integral approach is used to build a connection with Hovrava–Lifshitz gravity in 2 + 1 dimensions[240]. The spectral dimension, defined as the scaling exponent of the average return probability of diffusion processes (such as random walks), is used in causal dynamical triangulation to measure the effective dimension of the underlying geometry[241]. It can provide an interesting bridge to geometry induced by network-driven processes, for which one expects that this geometry characterizes the underlying diffusion manifold. More recently, a model[242] in which random graphs dynamically self-assemble into discrete manifold structures has been proposed as an alternative to approaches based on simplicial complexes and Regge calculus. The Ollivier curvature, defined for generic graphs — and similar in spirit to Ricci curvature — is used to discretize the Euclidean Einstein–Hilbert action and to provide a new ground for emergent time mechanisms[242].

In network science, a step forwards[231,232,243–245] in addressing the geometrogenesis problem has been to define models of growing random graphs and simplicial complexes. For a wide range of parameters, these models lead to an effective preferential attachment and, thus, heterogeneous degree distributions[243]. In addition, some growth processes can be mapped to trees, leading to emergent hyperbolic geometry in the resulting graphs[245]. For a more exhaustive introduction to the topic, we refer the interested reader to the review in REF.[232].

Graph curvature. Curvature is one of the most basic geometric notions, and a key player in the Einstein–Hilbert action, whose least-action variation leads to Einstein's equations in general relativity. It is thus not surprising that graph curvature appears in many flavours of geometrogenesis and combinatorial approaches to quantum gravity[242]. More surprising is that there is not one but many successful attempts to port the notion of curvature to the realm of networks, resulting in many non-equivalent definitions of graph curvature[105,246–252]. Unfortunately, none of these definitions of graph curvature is rigorously known to converge to any traditional curvature of smooth space in the continuum limit of any random graph ensemble, with the exception of Ollivier curvature of random geometric graphs recently shown to converge to Ricci curvature in any Riemannian manifold under some strong assumptions[253].

Nevertheless, many of these graph-curvature definitions have recently found applications in diverse applications such as differentiating cancer networks[254], characterizing human brain structural connectivity[172] and mesoscale characterization of complex networks based on Ollivier–Ricci curvature[255] and Ricci flow[256].

The topic is receiving increasing attention because combinatorial notions of network curvature have disclosed profound connections between network measures, such as the graph Laplacian, and exquisitely geometrical quantities such as the Laplace–Beltrami operator in Riemannian manifolds[257,258] or the Fisher–Rao metric in information geometry[259].

An important combinatorial definition of curvature that is directly applicable to networks, is Gromov's δ-hyperbolicity[88], which has been measured for a variety of real-world networks[260–263]. It is a rough measure of how far a metric space is from a tree[264]. It applies to any metric space, including the metric spaces of shortest-path distances and the latent spaces. Any hyperbolic space is also δ-hyperbolic[94], but a network is called δ-hyperbolic if its shortest-path metric space is such. This terminology often causes confusion because networks in the hyperbolic latent-space models discussed in this Review Article, which are often called random hyperbolic graphs, are actually unlikely to be δ-hyperbolic because their two different limits are not δ-hyperbolic[265,266]. However, at present, it is not exactly known how δ-hyperbolic the random hyperbolic graphs are — another open problem.

Topological data analysis. Another interesting bridge with topology has been established by generalizing networks to higher dimensions via simplicial complexes. Doing so allows for the application of persistent homology methods[267] from topological data analysis (TDA)[268]. Persistent homology relies on the filtration of a simplicial complex to uncover topological features that recur over multiple scales and are thus likely to represent some true features of the underlying space. The TDA in general and persistent homology in particular are vigorous research areas in data science that find applications in problems including spreading processes in networks[41] and the detection of geometric structure in neural activity[269]. For thorough reviews of advances in TDA, we refer the interested reader to REFS[270,271].

Taken together, the advances in network geometry offer a new theoretical framework to gain deep insights into the fundamental principles of complex systems and, more generally, into physical reality. It is not excluded that the existing results and future advances in this area will lead to fruitful cross-fertilization with other areas of physics.

Published online: 29 January 2021

1. Cimini, G. et al. The statistical physics of real-world networks. *Nat. Rev. Phys.* **1**, 58–71 (2019).
2. Watts, D. J. & Strogatz, S. H. Collective dynamics of 'small-world' networks. *Nature* **393**, 440–442 (1998).
3. Barabási, A.-L. & Albert, R. Emergence of scaling in random networks. *Science* **286**, 509–512 (1999).
4. Ravasz, E., Somera, A. L., Mongru, D. A., Oltvai, Z. N. & Barabási, A.-L. Hierarchical organization of modularity in metabolic networks. *Science* **297**, 1551–1555 (2002).
5. Dorogovtsev, S. N., Goltsev, A. V. & Mendes, J. F. F. Critical phenomena in complex networks. *Rev. Mod. Phys.* **80**, 1275–1335 (2008).
6. Gao, J., Buldyrev, S. V., Stanley, H. E. & Havlin, S. Networks formed from interdependent networks. *Nat. Phys.* **8**, 40–48 (2012).
7. D'Souza, R. M. & Nagler, J. Anomalous critical and supercritical phenomena in explosive percolation. *Nat. Phys.* **11**, 531–538 (2015).
8. Gao, J., Barzel, B. & Barabási, A.-L. Universal resilience patterns in complex networks. *Nature* **530**, 307–312 (2016).
9. Bianconi, G. Interdisciplinary and physics challenges of network theory. *Europhys. Lett.* **111**, 56001 (2015).
10. Estrada, E. *The Structure of Complex Networks: Theory and Applications* (Oxford Univ. Press, 2012).
11. Garlaschelli, D., Capocci, A. & Caldarelli, G. Self-organized network evolution coupled to extremal dynamics. *Nat. Phys.* **3**, 813–817 (2007).
12. Garlaschelli, D. & Loffredo, M. Generalized Bose–Fermi statistics and structural correlations in weighted networks. *Phys. Rev. Lett.* **102**, 038701 (2009).
13. Kalinin, N. et al. Self-organized criticality and pattern emergence through the lens of tropical geometry. *Proc. Natl Acad. Sci. USA* **115**, E8135–E8142 (2018).
14. Song, C., Havlin, S. & Makse, H. A. Self-similarity of complex networks. *Nature* **433**, 392–395 (2005).
15. Gallos, L. K., Song, C., Havlin, S. & Makse, H. A. Scaling theory of transport in complex biological networks. *Proc. Natl Acad. Sci. USA* **104**, 7746–7751 (2007).
16. Condamin, S., Bénichou, O., Tejedor, V., Voituriez, R. & Klafter, J. First-passage times in complex scale-invariant media. *Nature* **450**, 77–80 (2007).
17. Radicchi, F., Ramasco, J., Barrat, A. & Fortunato, S. Complex networks renormalization: flows and fixed points. *Phys. Rev. Lett.* **101**, 148701 (2008).
18. Rozenfeld, H. D., Song, C. & Makse, H. A. Small-world to fractal transition in complex networks: a renormalization group approach. *Phys. Rev. Lett.* **104**, 025701 (2010).

19. Song, C., Havlin, S. & Makse, H. A. Origins of fractality in the growth of complex networks. *Nat. Phys.* **2**, 275–281 (2006).
20. Serrano, M. Á., Krioukov, D. & Boguñá, M. Self-similarity of complex networks and hidden metric spaces. *Phys. Rev. Lett.* **100**, 078701 (2008).
21. Krioukov, D., Papadopoulos, F., Kitsak, M., Vahdat, A. & Boguñá, M. Hyperbolic geometry of complex networks. *Phys. Rev. E* **82**, 036106 (2010).
22. Sorokin, A. P. *Social Mobility* (Harper, 1927).
23. McFarland, D. D. & Brown, D. J. *Social Distance as a Metric: A Systematic Introduction to Smallest Space Analysis* 213–252 (John Wiley, 1973).
24. Hoff, P. D., Raftery, A. E. & Handcock, M. S. Latent space approaches to social network analysis. *J. Am. Stat. Assoc.* **97**, 1090–1098 (2002).
25. Boguñá, M., Krioukov, D. & Claffy, K. C. Navigability of complex networks. *Nat. Phys.* **5**, 74–80 (2009).
26. Gulyás, A., Bíró, J. J., Kőrösi, A., Rétvári, G. & Krioukov, D. Navigable networks as Nash equilibria of navigation games. *Nat. Commun.* **6**, 7651 (2015).
27. Allard, A. & Serrano, M. Á. Navigable maps of structural brain networks across species. *PLoS Comput. Biol.* **16**, e1007584 (2020).
28. Muscoloni, A. & Cannistraci, C. V. Navigability evaluation of complex networks by greedy routing efficiency. *Proc. Natl Acad. Sci. USA* **116**, 1468–1469 (2019).
29. Zuev, K., Boguñá, M., Bianconi, G. & Krioukov, D. Emergence of soft communities from geometric preferential attachment. *Sci. Rep.* **5**, 9421 (2015).
30. García-Pérez, G., Boguñá, M., Allard, A. & Serrano, M. Á. The hidden hyperbolic geometry of international trade: World Trade Atlas 1870–2013. *Sci. Rep.* **6**, 33441 (2016).
31. Wang, Z., Li, Q., Jin, F., Xiong, W. & Wu, Y. Hyperbolic mapping of complex networks based on community information. *Physica A* **455**, 104–119 (2016).
32. García-Pérez, G., Serrano, M. Á. & Boguñá, M. Soft communities in similarity space. *J. Stat. Phys.* **173**, 775–782 (2018).
33. Muscoloni, A. & Cannistraci, C. Leveraging the nonuniform PSO network model as a benchmark for performance evaluation in community detection and link prediction. *New J. Phys.* **20**, 063022 (2018).
34. García-Pérez, G., Boguñá, M. & Serrano, M. Á. Multiscale unfolding of real networks by geometric renormalization. *Nat. Phys.* **14**, 583–589 (2018).
35. Papadopoulos, F., Kitsak, M., Serrano, M. Á., Boguñá, M. & Krioukov, D. Popularity versus similarity in growing networks. *Nature* **489**, 537–540 (2012).
36. Zuev, K., Papadopoulos, F. & Krioukov, D. Hamiltonian dynamics of preferential attachment. *J. Phys. A* **49**, 105001 (2016).

37. Zheng, M., García-Pérez, G., Boguñá, M. & Serrano, M. A. Scaling up real networks by geometric branching growth. Preprint at https://arxiv.org/abs/1912.00704 (2019).
38. Krioukov, D. & Ostilli, M. Duality between equilibrium and growing networks. *Phys. Rev. E* **88**, 022808 (2013).
39. Coifman, R. R. et al. Geometric diffusions as a tool for harmonic analysis and structure definition of data: diffusion maps. *Proc. Natl Acad. Sci. USA* **102**, 7426–7431 (2005).
40. Brockmann, D. & Helbing, D. The hidden geometry of complex, network-driven contagion phenomena. *Science* **342**, 1337–1342 (2013).
41. Taylor, D. et al. Topological data analysis of contagion maps for examining spreading processes on networks. *Nat. Commun.* **6**, 7723 (2015).
42. De Domenico, M. Diffusion geometry unravels the emergence of functional clusters in collective phenomena. *Phys. Rev. Lett.* **118**, 168301 (2017).
43. Hens, C., Harush, U., Haber, S., Cohen, R. & Barzel, B. Spatiotemporal signal propagation in complex networks. *Nat. Phys.* **10**, 403–412 (2019).
44. Feder, J. *Fractals* (Springer Science & Business Media, 2013).
45. Frisch, U. & Kolmogorov, A. N. *Turbulence: The Legacy of AN Kolmogorov* (Cambridge Univ. Press, 1995).
46. Cardy, J. *Scaling and Renormalization in Statistical Physics* Vol. 5 (Cambridge Univ. Press, 1996).
47. Lesne, A. & Laguës, M. *Scale Invariance: From Phase Transitions to Turbulence* (Springer Science & Business Media, 2011).
48. Bak, P. *How Nature Works: The Science of Self-organized Criticality* (Springer Science & Business Media, 2013).
49. Carlson, J. M. & Doyle, J. Complexity and robustness. *Proc. Natl Acad. Sci. USA* **99**, 2538–2545 (2002).
50. Bollobás, B. *Modern Graph Theory* Vol. 184 (Springer Science & Business Media, 2013).
51. Chung, F. & Lu, L. The average distances in random graphs with given expected degrees. *Proc. Natl Acad. Sci. USA* **99**, 15879–82 (2002).
52. Cohen, R. & Havlin, S. Scale-free networks are ultrasmall. *Phys. Rev. Lett.* **90**, 058701 (2003).
53. Dorogovtsev, S. N., Mendes, J. F. F. & Samukhin, A. N. Metric structure of random networks. *Nucl. Phys. B* **653**, 307–422 (2003).
54. Mandelbrot, B. B. *The Fractal Geometry of Nature* Vol. 2 (WH Freeman, 1982).
55. Harary, F. *Graph Theory* (Addison-Wesley, 1994).
56. Wiener, H. Structural determination of paraffin boiling points. *J. Am. Chem. Soc.* **69**, 17–20 (1947).

57. Havlin, S., Trus, B. & Stanley, H. Cluster-growth model for branched polymers that are "chemically linear". *Phys. Rev. Lett.* **53**, 1288–1291 (1984).

58. Wilson, K. G. The renormalization group and critical phenomena. *Rev. Mod. Phys.* **55**, 583–600 (1983).

59. Efrati, E., Wang, Z., Kolan, A. & Kadanoff, L. P. Real-space renormalization in statistical mechanics. *Rev. Mod. Phys.* **86**, 647 (2014).

60. Gallos, L. K., Song, C. & Makse, H. A. Scaling of degree correlations and its influence on diffusion in scale-free networks. *Phys. Rev. Lett.* **100**, 248701 (2008).

61. Bunde, A. & Havlin, S. *Fractals and Disordered Systems* (Springer Science & Business Media, 2012).

62. Goh, K.-I., Salvi, G., Kahng, B. & Kim, D. Skeleton and fractal scaling in complex networks. *Phys. Rev. Lett.* **96**, 018701 (2006).

63. Kim, J. et al. Fractality in complex networks: critical and supercritical skeletons. *Phys. Rev. E* **75**, 016110 (2007).

64. Yook, S.-H., Radicchi, F. & Meyer-Ortmanns, H. Self-similar scale-free networks and disassortativity. *Phys. Rev. E* **72**, 045105 (2005).

65. Galvão, V. et al. Modularity map of the network of human cell differentiation. *Proc. Natl Acad. Sci. USA* **107**, 5750–5755 (2010).

66. Newman, M. E. J. Modularity and community structure in networks. *Proc. Natl Acad. Sci. USA* **103**, 8577–8582 (2006).

67. Fortunato, S. Community detection in graphs. *Phys. Rep.* **486**, 75–174 (2010).

68. Stanley, H. E. Scaling, universality, and renormalization: three pillars of modern critical phenomena. *Rev. Mod. Phys.* **71**, S358–S366 (1999).

69. Radicchi, F., Barrat, A., Fortunato, S. & Ramasco, J. Renormalization flows in complex networks. *Phys. Rev. E* **79**, 026104 (2009).

70. Stanley, H. E. *Introduction to Phase Transitions and Critical Phenomena* (Oxford Univ. Press, 1971).

71. Kleinberg, J. Navigation in a small world. *Nature* **406**, 845 (2000).

72. Viswanathan, G. M. et al. Optimizing the success of random searches. *Nature* **401**, 911–914 (1999).

73. Strogatz, S. H. Complex systems: Romanesque networks. *Nature* **433**, 365–366 (2005).

74. Dorogovtsev, S. N. & Mendes, J. F. F. *Evolution of Networks: From Biological Nets to the Internet and WWW* (Oxford Univ. Press, 2003).

75. Rozenfeld, H. D., Gallos, L. K., Song, C. & Makse, H. A. in *Encyclopedia of Complexity and Systems Science* (ed. Meyers R.) 3924–3943 (Springer, 2009).

76. Kitano, H. Systems biology: a brief overview. *Science* **295**, 1662–1664 (2002).

77. Jin, Y., Turaev, D., Weinmaier, T., Rattei, T. & Makse, H. A. The evolutionary dynamics of protein–protein interaction networks inferred from the reconstruction of ancient networks. *PLoS ONE* **8**, e58134 (2013).

78. Villani, C. *Optimal Transport: Old and New* Vol. 338 (Springer Science & Business Media, 2008).

79. Ben-Avraham, D. & Havlin, S. *Diffusion and Reactions in Fractals and Disordered Systems* (Cambridge Univ. Press, 2000).

80. Haynes, C. P. & Roberts, A. P. Generalization of the fractal Einstein law relating conduction and diffusion on networks. *Phys. Rev. Lett.* **103**, 020601 (2009).

81. Masuda, N., Porter, M. A. & Lambiotte, R. Random walks and diffusion on networks. *Phys. Rep.* **716**, 1–58 (2017).

82. Gallos, L. K., Potiguar, F. Q., Andrade Jr, J. S. & Makse, H. A. IMDb network revisited: unveiling fractal and modular properties from a typical small-world network. *PLoS ONE* **8**, e66443 (2013).

83. Gallos, L. K., Makse, H. A. & Sigman, M. A small world of weak ties provides optimal global integration of self-similar modules in functional brain networks. *Proc. Natl Acad. Sci. USA* **109**, 2825–2830 (2012).

84. Avena-Koenigsberger, A., Misic, B. & Sporns, O. Communication dynamics in complex brain networks. *Nat. Rev. Neurosci.* **19**, 17–33 (2017).

85. Gallos, L. K., Song, C. & Makse, H. A. A review of fractality and self-similarity in complex networks. *Physica A* **386**, 686–691 (2007).

86. Bloch, A. On methods for the construction of networks dual to non-planar networks. *Proc. Phys. Soc.* **58**, 677–694 (1946).

87. Estrada, E. The communicability distance in graphs. *Linear Algebra Appl.* **436**, 4317–4328 (2012).

88. Gromov, M. in *Essays in Group Theory* (ed. Gersten S. M.) 75–263 (Mathematical Sciences Research Institute Publications Vol. 8, Springer, 1987).

89. Nekrashevych, V. Hyperbolic spaces from self-similar group actions. *Algebra Discret. Math.* **2**, 77–86 (2003).

90. Nekrashevych, V. *Self-Similar Groups* (Mathematical Surveys and Monographs Vol. 117, American Mathematical Society, 2005).

91. Furstenberg, H. *Ergodic Theory and Fractal Geometry* Vol. 120 (American Mathematical Society, 2014).

92. Furstenberg, H. & Weiss, B. Markov processes and Ramsey theory for trees. *Comb. Probab. Comput.* **12**, 547–563 (2003).

93. Dorogovtsev, S. N. & Mendes, J. F. F. Evolution of networks. *Adv. Phys.* **51**, 1079–1187 (2002).

94. Buyalo, S. & Schroeder, V. *Elements of Asymptotic Geometry* (European Mathematical Society Publishing House, 2007).

95. Grigorchuk, R., Nekrashevych, V. & Šunić, Z. *From Self-Similar Groups to Self-Similar Sets and Spectra* 175–207 (Birkhäuser, 2015).

96. Boguñá, M. & Krioukov, D. Navigating ultrasmall worlds in ultrashort time. *Phys. Rev. Lett.* **102**, 058701 (2009).

97. Boguñá, M., Papadopoulos, F. & Krioukov, D. Sustaining the Internet with hyperbolic mapping. *Nat. Commun.* **1**, 62 (2010).

98. Penrose, M. *Random Geometric Graphs* (Oxford Univ. Press, 2003).

99. Boguñá, M., Krioukov, D., Almagro, P. & Serrano, M. Ã. Small worlds and clustering in spatial networks. *Phys. Rev. Res.* **2**, 023040 (2020).

100. van der Hoorn, P., Lippner, G. & Krioukov, D. Sparse maximum-entropy random graphs with a given power-law degree distribution. *J. Stat. Phys.* **173**, 806–844 (2018).

101. Voitalov, I., van der Hoorn, P., van der Hofstad, R. & Krioukov, D. Scale-free networks well done. *Phys. Rev. Res.* **1**, 033034 (2019).

102. Cannon, J., Floyd, W., Kenyon, R. & Parry, W. *Hyperbolic Geometry* 59–116 (MSRI, 1997).

103. Matoušek, J. in *Lectures on Discrete Geometry. Graduate Texts in Mathematics* Vol 212. (ed. Matoušek J.) Ch. 15 (Springer, 2002).

104. Munzner, T. Exploring large graphs in 3D hyperbolic space. *IEEE Comput. Graph. Appl.* **18**, 18–23 (1998).

105. Aste, T., Dimatteo, T. & Hyde, S. Complex networks on hyperbolic surfaces. *Physica A* **346**, 20–26 (2005).

106. Lohsoonthorn, P. *Hyperbolic Geometry of Networks*. PhD thesis, USC (2003).

107. Jonckheere, E., Lohsoonthorn, P. & Bonahon, F. Scaled Gromov hyperbolic graphs. *J. Graph. Theory* **57**, 157–180 (2008).

108. Kleinberg, R. Geographic routing using hyperbolic space. In *IEEE INFOCOM 2007 - 26th IEEE Int. Conf. Comput. Commun.* 1902–1909 (IEEE, 2007).

109. Ratcliffe, J. *Foundations of Hyperbolic Manifolds* (Springer, 2006).

110. Dall, J. & Christensen, M. Random geometric graphs. *Phys. Rev. E* **66**, 016121 (2002).

111. Krioukov, D. et al. Network cosmology. *Sci. Rep.* **2**, 793 (2012).

112. Allard, A., Serrano, M. Ã., García-Pêrez, G. & Boguñá, M. The geometric nature of weights in real complex networks. *Nat. Commun.* **8**, 14103 (2017).

113. Kleineberg, K.-K., Boguñá, M., Ángeles Serrano, M. & Papadopoulos, F. Hidden geometric correlations in real multiplex networks. *Nat. Phys.* **12**, 1076–1081 (2016).

114. Kleineberg, K.-K., Buzna, L., Papadopoulos, F., Boguñá, M. & Serrano, M. A. Geometric correlations mitigate the extreme vulnerability of multiplex networks against targeted attacks. *Phys. Rev. Lett.* **118**, 218301 (2017).

115. Muscoloni, A. & Cannistraci, C. V. A nonuniform popularity-similarity optimization (nPSO) model to efficiently generate realistic complex networks with communities. *New J. Phys.* **20**, 052002 (2018).

116. Maldacena, J. The large *N* limit of superconformal field theories and supergravity. *Adv. Theor. Math. Phys.* **2**, 231–252 (1998).

117. Gugelmann, L., Panagiotou, K. & Peter, U. *Random Hyperbolic Graphs: Degree Sequence and Clustering* 573–585 (Springer, 2012).

118. Fountoulakis, N. On a geometrization of the Chung–Lu model for complex networks. *J. Complex Netw.* **3**, 361–387 (2015).

119. Candellero, E. & Fountoulakis, N. Clustering and the hyperbolic geometry of complex networks. *Internet Math.* **12**, 2–53 (2016).

120. Bode, M., Fountoulakis, N. & Müller, T. The probability of connectivity in a hyperbolic model of complex networks. *Random Struct. Algorithms* **49**, 65–94 (2016).

121. Bringmann, K., Keusch, R., Lengler, J., Maus, Y. & Molla, A. R. Greedy routing and the algorithmic small-world phenomenon. In *Proc. ACM Symp. Princ. Distrib. Comput. - PODC'17* 371–380 (ACM Press, 2017).

122. Abdullah, M. A., Fountoulakis, N. & Bode, M. Typical distances in a geometric model for complex networks. *Internet Math.* https://doi.org/10.24166/im.13.2017 (2017).

123. Bläsius, T., Friedrich, T. & Krohmer, A. Cliques in hyperbolic random graphs. *Algorithmica* **80**, 2324–2344 (2018).

124. Fountoulakis, N. & Müller, T. Law of large numbers for the largest component in a hyperbolic model of complex networks. *Ann. Appl. Probab.* **28**, 607–650 (2018).

125. Friedrich, T. & Krohmer, A. On the diameter of hyperbolic random graphs. *SIAM J. Discret. Math.* **32**, 1314–1334 (2018).

126. Kiwi, M. & Mitsche, D. Spectral gap of random hyperbolic graphs and related parameters. *Ann. Appl. Probab.* **28**, 941–989 (2018).

127. Bringmann, K., Keusch, R. & Lengler, J. Geometric inhomogeneous random graphs. *Theor. Comput. Sci.* **760**, 35–54 (2019).

128. Müller, T. & Staps, M. The diameter of KPKVB random graphs. *Adv. Appl. Probab.* **51**, 358–377 (2019).

129. Papadopoulos, F., Psomas, C. & Krioukov, D. Network mapping by replaying hyperbolic growth. *IEEE/ACM Trans. Netw.* **23**, 198–211 (2015).

130. Papadopoulos, F., Aldecoa, R. & Krioukov, D. Network geometry inference using common neighbors. *Phys. Rev. E* **92**, 022807 (2015).

131. Blasius, T., Friedrich, T., Krohmer, A. & Laue, S. Efficient embedding of scale-free graphs in the hyperbolic plane. *IEEE/ACM Trans. Netw.* **26**, 920–933 (2018).

132. Muscoloni, A., Thomas, J. M., Ciucci, S., Bianconi, G. & Cannistraci, C. V. Machine learning meets complex networks via coalescent embedding in the hyperbolic space. *Nat. Commun.* **8**, 1615 (2017).

133. Alanis-Lobato, G., Mier, P. & Andrade-Navarro, M. A. Efficient embedding of complex networks to hyperbolic space via their Laplacian. *Sci. Rep.* **6**, 30108 (2016).

134. Wang, Z., Wu, Y., Li, Q., Jin, F. & Xiong, W. Link prediction based on hyperbolic mapping with community structure for complex networks. *Physica A* **450**, 609–623 (2016).

135. Muscoloni, A. & Cannistraci, C. V. Minimum curvilinear automata with similarity attachment for network embedding and link prediction in the hyperbolic space. Preprint at https://arxiv.org/abs/1802.01183 (2018).

136. Alanis-Lobato, G., Mier, P. & Andrade-Navarro, M. A. Manifold learning and maximum likelihood estimation for hyperbolic network embedding. *Appl. Netw. Sci.* **1**, 10 (2016).

137. Garcia-Perez, G., Allard, A., Serrano, M. A. & Boguna, M. Mercator: uncovering faithful hyperbolic embeddings of complex networks. *New J. Phys.* **21**, 123033 (2019).

138. Kitsak, M., Voitalov, I. & Krioukov, D. Link prediction with hyperbolic geometry. *Phys. Rev. Res.* **2**, 043113 (2020).

139. Serrano, M. Ã., Boguñá, M. & Sagués, F. Uncovering the hidden geometry behind metabolic networks. *Mol. Biosyst.* **8**, 843–850 (2012).

140. Kleineberg, K.-K. Metric clusters in evolutionary games on scale-free networks. *Nat. Commun.* **8**, 1888 (2017).

141. García-Pérez, G., Aliakbarisani, R., Ghasemi, A. & Serrano, M. Ã. Precision as a measure of predictability of missing links in real networks. *Phys. Rev. E* **101**, 052318 (2020).

142. Kerrache, S., Alharbi, R. & Benhidour, H. A scalable similarity–popularity link prediction method. *Sci. Rep.* **10**, 6394 (2020).

143. Voitalov, I., Aldecoa, R., Wang, L. & Krioukov, D. Geohyperbolic routing and addressing schemes. *ACM SIGCOMM Comput. Commun. Rev* **47**, 11–18 (2017).

144. Zheng, M., Allard, A., Hagmann, P., Alemán-Gómez, Y. & Serrano, M. Ã. Geometric renormalization unravels self-similarity of the multiscale human connectome. *Proc. Natl Acad. Sci. USA* **117**, 20244–20253 (2020).

145. Cacciola, A. et al. Coalescent embedding in the hyperbolic space unsupervisedly discloses the hidden geometry of the brain. Preprint at https://arxiv.org/abs/1705.04192 (2017).

146. Faqeeh, A., Osat, S. & Radicchi, F. Characterizing the analogy between hyperbolic embedding and

community structure of complex networks. *Phys. Rev. Lett.* **121**, 098301 (2018).

147. Boguñá, M., Pastor-Satorras, R. & Vespignani, A. Cut-offs and finite size effects in scale-free networks. *Eur Phys. J. B* **38**, 205–209 (2004).

148. Catanzaro, M., Boguñá, M. & Pastor-Satorras, R. Generation of uncorrelated random scale-free networks. *Phys. Rev. E* **71**, 027103 (2005).

149. Korman, A. & Peleg, D. *Dynamic Routing Schemes for General Graphs* 619–630 (Lecture Notes in Computer Science Vol. 4051, Springer, 2006).

150. Serrano, M. Á., Krioukov, D. & Boguñá, M. Percolation in self-similar networks. *Phys. Rev. Lett.* **106**, 048701 (2011).

151. Cohen, R., Erez, K., Ben-Avraham, D. & Havlin, S. Resilience of the internet to random breakdowns. *Phys. Rev. Lett.* **85**, 4626–4628 (2000).

152. Pastor-Satorras, R. & Vespignani, A. Epidemic spreading in scale-free networks. *Phys. Rev. Lett.* **86**, 3200–3203 (2001).

153. Bianconi, G. Mean field solution of the Ising model on a Barabási–Albert network. *Phys. Lett. A* **303**, 166–168 (2002).

154. Dorogovtsev, S. N., Goltsev, A. V. & Mendes, J. F. F. Ising model on networks with an arbitrary distribution of connections. *Phys. Rev. E* **66**, 016104 (2002).

155. Leone, M., Vázquez, A., Vespignani, A. & Zecchina, R. Ferromagnetic ordering in graphs with arbitrary degree distribution. *Eur. Phys. J. B* **28**, 191–197 (2002).

156. Kadanoff, L. P. *Statistical Physics: Statics, Dynamics and Renormalization* (World Scientific, 2000).

157. Arenas, A., Díaz-Guilera, A., Kurths, J., Moreno, Y. & Zhou, C. Synchronization in complex networks. *Phys. Rep.* **469**, 93–153 (2008).

158. van den Heuvel, M. P., Kahn, R. S., Goni, J. & Sporns, O. High-cost, high-capacity backbone for global brain communication. *Proc. Natl Acad. Sci. USA* **109**, 11372–11377 (2012).

159. Goñi, J. et al. Exploring the morphospace of communication efficiency in complex networks. *PLoS ONE* **8**, e58070 (2013).

160. Fornito, A., Zalesky, A. & Breakspear, M. Graph analysis of the human connectome: promise, progress, and pitfalls. *Neuroimage* **80**, 426–444 (2013).

161. Mišić, B., Sporns, O. & McIntosh, A. R. Communication efficiency and congestion of signal traffic in large-scale brain networks. *PLoS Comput. Biol.* **10**, e1003427 (2014).

162. Roberts, J. A. et al. The contribution of geometry to the human connectome. *Neuroimage* **124**, 379–393 (2016).

163. Avena-Koenigsberger, A. et al. Path ensembles and a tradeoff between communication efficiency and resilience in the human connectome. *Brain Struct. Funct.* **222**, 603–618 (2017).

164. Seguin, C., van den Heuvel, M. P. & Zalesky, A. Navigation of brain networks. *Proc. Natl Acad. Sci. USA* **115**, 6297–6302 (2018).

165. Tadić, B., Andjelković, M. & Šuvakov, M. Origin of hyperbolicity in brain-to-brain coordination networks. *Front. Phys.* **6**, 7 (2018).

166. Avena-Koenigsberger, A. et al. A spectrum of routing strategies for brain networks. *PLoS Comput. Biol.* **15**, e1006833 (2019).

167. Wang, X. et al. Synchronization lag in post stroke: relation to motor function and structural connectivity. *Netw. Neurosci.* **3**, 1121–1140 (2019).

168. Betzel, R. F. et al. Generative models of the human connectome. *Neuroimage*, **124** 1054–1064 (2015).

169. Horvát, S. et al. Spatial embedding and wiring cost constrain the functional layout of the cortical network of rodents and primates. *PLoS Biol.* **14**, e1002512 (2016).

170. Stiso, J. & Bassett, D. S. Spatial embedding imposes constraints on neuronal network architectures. *Trends Cogn. Sci.* **22**, 1127–1142 (2018).

171. Allen, Q. Y. et al. The intrinsic geometry of the human brain connectome. *Brain Inform.* **2**, 197–210 (2015).

172. Farooq, H., Chen, Y., Georgiou, T. T., Tannenbaum, A. & Lenglet, C. Network curvature as a hallmark of brain structural connectivity. *Nat. Commun.* **10**, 4937 (2019).

173. Assaf, Y., Bouznach, A., Zomet, O., Marom, A. & Yovel, Y. Conservation of brain connectivity and wiring across the mammalian class. *Nat. Neurosci.* **23**, 805–808 (2020).

174. Nickel, M. & Kiela, D. Poincaré embeddings for learning hierarchical representations. *Adv. Neural Inf. Process. Syst.* (2017).

175. Dhingra, B., Shallue, C. J., Norouzi, M., Dai, A. M. & Dahl, G. E. Embedding text in hyperbolic spaces. In *Proc. Twelfth Work Graph-Based Methods Nat. Lang. Process* 59–69 (Association for Computational Linguistics, 2018).

176. Ganea, O.-E., Bécigneul, G. & Hofmann, T. Hyperbolic entailment cones for learning hierarchical embeddings. In *Proc 35th Int. Conf. Mach. Learn.* (eds Dy, J., & Krause, A.) 1646–1655 (PMLR, 2018).

177. Ganea, O.-E., Bécigneul, G. & Hofmann, T. Hyperbolic neural networks. *Adv. Neural Inf. Process. Syst.* (2018).

178. Nickel, M. & Kiela, D. Learning continuous hierarchies in the Lorentz model of hyperbolic geometry. In *Int. Conf. Mach. Learn.* (eds Dy, J., & Krause, A.) 3776–3785 (PMLR, 2018).

179. Ovinnikov, I. Poincaré Wasserstein autoencoder. Preprint at https://arxiv.org/abs/1901.01427 (2019).

180. Sala, F. et al. Representation tradeoffs for hyperbolic embeddings. In *Int. Conf. Mach. Learn.* (eds Dy, J., & Krause, A.) 4460–4469 (PMLR, 2018).

181. Gulcehre, C. et al. Hyperbolic attention networks. In *Int. Conf. Learn. Represent ICLR 2019* (OpenReview.net, 2019).

182. Chami, I., Ying, R., Ré, C. & Leskovec, J. Hyperbolic graph convolutional neural networks. In *Adv. Neural Inf. Process. Syst.* (Wallach, H. et al) 4868–4879 (2019).

183. Liu, Q., Nickel, M. & Kiela, D. Hyperbolic graph neural networks. In *Adv. Neural Inf. Process. Syst.* (Wallach, H. et al) 8230–8241 (2019).

184. Suzuki, A., Wang, J., Tian, F., Nitanda, A. & Yamanishi, K. Hyperbolic ordinal embedding. In *Proc. Elev. Asian Conf. Mach. Learn* (Lee, W. S., & Suzuki, T.) 1065–1080 (PMLR, 2019).

185. Tifrea, A., Bécigneul, G. & Ganea, O.-E. Poincaré GloVe: hyperbolic word embeddings. In *Int. Conf. Learn. Represent* (OpenReview.net, 2019).

186. Orsini, C. et al. Quantifying randomness in real networks. *Nat. Commun.* **6**, 8627 (2015).

187. Gu, W., Tandon, A., Ahn, Y.-Y. & Radicchi, F. Defining and identifying the optimal embedding dimension of networks. Preprint at https://arxiv.org/abs/2004.09928 (2020).

188. Chaudhari, P. et al. Entropy-SGD: biasing gradient descent into wide valleys. *J. Stat. Mech. Theor. Exp.* **2019**, 124018 (2019).

189. Krioukov, D. Clustering implies geometry in networks. *Phys. Rev. Lett.* **116**, 208302 (2016).

190. Holme, P. & Saramäki, J. Temporal networks. *Phy. Rep.* **519**, 97–125 (2012).

191. Kallenberg, O. *Probabilistic Symmetries and Invariance Principles* (Springer, 2005).

192. Lovász, L. *Large Networks and Graph Limits* (American Mathematical Society, 2012).

193. Orbanz, P. & Roy, D. M. Bayesian models of graphs, arrays and other exchangeable random structures. *IEEE Trans. Pattern Anal. Mach. Intell.* **37**, 437–461 (2015).

194. Aldous, D. J. Representations for partially exchangeable arrays of random variables. *J. Multivar. Anal.* **11**, 581–598 (1981).

195. Hoover, D. N. *Relations on Probability Spaces and Arrays of Random Variables* Technical Report (Institute for Advanced Study, 1979).

196. Caron, F. & Fox, E. B. Sparse graphs using exchangeable random measures. *J. R. Stat. Soc. Ser. B* **79**, 1295–1366 (2017).

197. Veitch, V. & Roy, D. M. Sampling and estimation for (sparse) exchangeable graphs. *Ann. Stat.* **47**, 3274–3299 (2019).

198. Borgs, C., Chayes, J. T., Cohn, H. & Zhao, Y. An *L*ᵖ theory of sparse graph convergence I: Limits, sparse random graph models, and power law distributions. *Trans. Am. Math. Soc.* **372**, 3019–3062 (2019).

199. Janson, S. On edge exchangeable random graphs. *J. Stat. Phys.* **173**, 448–484 (2018).

200. Muscoloni, A. & Cannistraci, C. V. Local-ring network automata and the impact of hyperbolic geometry in complex network link-prediction. Preprint at https://arxiv.org/abs/1707.09496 (2017).

201. Klein, D. J. & Randić, M. Resistance distance. *J. Math. Chem.* **12**, 81–95 (1993).

202. Babić, D., Klein, D., Lukovits, I., Nikolić, S. & Trinajstić, N. Resistance-distance matrix: a computational algorithm and its application. *Int. J. Quantum Chem.* **90**, 166–176 (2002).

203. McRae, B. H. Isolation by resistance. *Evolution* **60**, 1551–1561 (2006).

204. Luxburg, U. V., Radl, A. & Hein, M. Getting lost in space: large sample analysis of the resistance distance. *Adv. Neural Inf. Process. Syst.* **23**, 2622–2630 (2010).

205. Estrada, E. Complex networks in the euclidean space of communicability distances. *Phys. Rev. E* **85**, 066122 (2012).

206. Estrada, E., Sánchez-Lirola, M. & De La Peña, J. A. Hyperspherical embedding of graphs and networks in communicability spaces. *Discret. Appl. Math.* **176**, 53–77 (2014).

207. Estrada, E. & Hatano, N. Communicability angle and the spatial efficiency of networks. *SIAM Rev.* **58**, 692–715 (2016).

208. Akbarzadeh, M. & Estrada, E. Communicability geometry captures traffic flows in cities. *Nat. Hum. Behav.* **2**, 645–652 (2018).

209. Estrada, E. Communicability geometry of multiplexes. *New J. Phys.* **21**, 015004 (2018).

210. De Domenico, M., Granell, C., Porter, M. A. & Arenas, A. The physics of spreading processes in multilayer networks. *Nat. Phys.* **12**, 901–906 (2016).

211. Estrada, E., Hatano, N. & Benzi, M. The physics of communicability in complex networks. *Phys. Rep.* **514**, 89–119 (2012).

212. Chebotarev, P. A class of graph–geodetic distances generalizing the shortest-path and the resistance distances. *Discret. Appl. Math.* **159**, 295–302 (2011).

213. Chebotarev, P. The walk distances in graphs. *Discret. Appl. Math.* **160**, 1484–1500 (2012).

214. Iannelli, F., Koher, A., Brockmann, D., Hoevel, P. & Sokolov, I. M. Effective distances for epidemics spreading on complex networks. *Phys. Rev. E* **95**, 012313 (2016).

215. Barthélemy, M. Spatial networks. *Phys. Rep.* **499**, 1–101 (2011).

216. Bonamassa, I., Gross, B., Danziger, M. M. & Havlin, S. Critical stretching of mean-field regimes in spatial networks. *Phys. Rev.Lett.* **123**, 088301 (2019).

217. Bertagnolli, G., Agostinelli, C. & Domenico, M. D. Network depth: identifying median and contours in complex networks. *J. Complex Netw.* **8**, cnz041 (2019).

218. Bertagnolli, G. & De Domenico, M. Diffusion geometry of multiplex and interdependent systems. Preprint at https://arxiv.org/abs/2006.13032 (2020).

219. De Domenico, M. et al. Mathematical formulation of multi-layer networks. *Phys. Rev. X* **3**, 041022 (2013).

220. De Domenico, M., Solé-Ribalta, A., Gómez, S. & Arenas, A. Navigability of interconnected networks under random failures. *Proc. Natl Acad. Sci. USA* **111**, 8351–8356 (2014).

221. Ravasz, E. & Barabási, A.-L. Hierarchical organization in complex networks. *Phys. Rev. E* **67**, 026112 (2003).

222. Corominas-Murtra, B., Goñi, J., Solé, R. V. & Rodríguez-Caso, C. On the origins of hierarchy in complex networks. *Proc. Natl Acad. Sci. USA* **110**, 13316–13321 (2013).

223. Newman, M. E. J., Strogatz, S. H. & Watts, D. J. Random graphs with arbitrary degree distributions and their applications. *Phys. Rev. E* **64**, 26118 (2001).

224. Dorogovtsev, S. N., Mendes, J. F. F. & Samukhin, A. N. Giant strongly connected component of directed networks. *Phys. Rev. E* **64**, 025101 (2001).

225. Seidman, S. B. Network structure and minimum degree. *Soc. Netw.* **5**, 269–287 (1983).

226. Dorogovtsev, S. N., Goltsev, A. V. & Mendes, J. F. F. *k*-core organization of complex networks. *Phys. Rev. Lett.* **96**, 040601 (2006).

227. Holme, P. Core–periphery organization of complex networks. *Phys. Rev. E* **72**, 046111 (2005).

228. Rombach, M. P., Porter, M. A., Fowler, J. H. & Mucha, P. J. Core–periphery structure in networks. *SIAM J. Appl. Math.* **74**, 167–190 (2014).

229. Papadopoulos, F., Krioukov, D., Boguna, M. & Vahdat, A. Greedy forwarding in dynamic scale-free networks embedded in hyperbolic metric spaces. In *2010 Proc IEEE INFOCOM* 1–9 (IEEE, 2010).

230. Cannistraci, C. V. & Muscoloni, A. Geometrical congruence and efficient greedy navigability of complex networks. Preprint at https://arxiv.org/abs/2005.13255 (2020).

231. Wu, Z., Menichetti, G., Rahmede, C. & Bianconi, G. Emergent complex network geometry. *Sci. Rep.* **5**, 10073 (2015).

232. Mulder, D. & Bianconi, G. Network geometry and complexity. *J. Stat. Phys.* **173**, 783–805 (2018).

233. Rideout, D. & Wallden, P. Spacelike distance from discrete causal order. *Class. Quantum Gravity* **26**, 155013 (2009).

234. Dowker, F. Spacetime discreteness, Lorentz invariance and locality. *J. Phys. Conf. Ser.* **306**, 012016 (2011).

235. Konopka, T., Markopoulou, F. & Severini, S. Quantum graphity: a model of emergent locality. *Phys. Rev. D* **77**, 104029 (2008).

236. Ambjørn, J., Jurkiewicz, J. & Loll, R. The spectral dimension of the universe is scale dependent. *Phys. Rev. Lett.* **95**, 171301 (2005).

237. Rovelli, C. & Speziale, S. On the geometry of loop quantum gravity on a graph. *Phys. Rev. D* **82**, 44018 (2010).

238. Grüber, D., Sahlmann, H. & Zilker, T. Geometry and entanglement entropy of surfaces in loop quantum gravity. *Phys. Rev. D* **98**, 066009 (2018).

239. Ambjørn, J., Jordan, S., Jurkiewicz, J. & Loll, R. Second-order phase transition in causal dynamical triangulations. *Phys. Rev. Lett.* **107**, 211303 (2011).

240. Sotiriou, T. P., Visser, M. & Weinfurtner, S. Spectral dimension as a probe of the ultraviolet continuum regime of causal dynamical triangulations. *Phys. Rev. Lett.* **107**, 131303 (2011).

241. Loll, R. Quantum gravity from causal dynamical triangulations: a review. *Class. Quantum Grav.* **37**, 013002 (2020).

242. Kelly, C., Trugenberger, C. A. & Biancalana, F. Self-assembly of geometric space from random graphs. *Class. Quantum Gravity* **36**, 125012 (2019).

243. Bianconi, G. & Rahmede, C. Complex quantum network manifolds in dimension $d > 2$ are scale-free. *Sci. Rep.* **5**, 13979 (2015).

244. Bianconi, G. & Rahmede, C. Network geometry with flavor: from complexity to quantum geometry. *Phys. Rev. E* **93**, 032315 (2016).

245. Bianconi, G. & Rahmede, C. Emergent hyperbolic network geometry. *Sci. Rep.* **7**, 41974 (2017).

246. Higuchi, Y. Combinatorial curvature for planar graphs. *J. Graph. Theor.* **38**, 220–229 (2001).

247. Ollivier, Y. Ricci curvature of Markov chains on metric spaces. *J. Funct. Anal.* **256**, 810–864 (2009).

248. Lin, Y., Lu, L. & Yau, S.-T. Ricci curvature of graphs. *Tohoku Math. J. Sec. Ser.* **63**, 605–627 (2011).

249. Sreejith, R., Mohanraj, K., Jost, J., Saucan, E. & Samal, A. Forman curvature for complex networks. *J. Stat. Mech. Theor. Exp.* **2016**, 063206 (2016).

250. Sreejith, R., Jost, J., Saucan, E. & Samal, A. Systematic evaluation of a new combinatorial curvature for complex networks. *Chaos Solitons Fractals* **101**, 50–67 (2017).

251. Samal, A. et al. Comparative analysis of two discretizations of Ricci curvature for complex networks. *Sci. Rep.* **8**, 8650 (2018).

252. Prokhorenkova, L., Samosvat, E. & van der Hoorn, P. *Global Graph Curvature* Vol. 2, 16–35 (Springer International Publishing, 2020).

253. van der Hoorn, P., Cunningham, W. J., Lippner, G., Trugenberger, C. & Krioukov, D. Ollivier–Ricci curvature convergence in random geometric graphs. Preprint at https://arxiv.org/abs/2008.01209 (2020).

254. Sandhu, R. et al. Graph curvature for differentiating cancer networks. *Sci. Rep.* **5**, 12323 (2015).

255. Sia, J., Jonckheere, E. & Bogdan, P. Ollivier–ricci curvature-based method to community detection in complex networks. *Sci. Rep.* **9**, 9800 (2019).

256. Ni, C.-C., Lin, Y.-Y., Luo, F. & Gao, J. Community detection on networks with Ricci flow. *Sci. Rep.* **9**, 1–12 (2019).

257. Robles-Kelly, A. & Hancock, E. R. A Riemannian approach to graph embedding. *Pattern Recognit.* **40**, 1042–1056 (2007).

258. Majid, S. Noncommutative Riemannian geometry on graphs. *J. Geom. Phys.* **69**, 74–93 (2013).

259. Franzosi, R., Felice, D., Mancini, S. & Pettini, M. Riemannian-geometric entropy for measuring network complexity. *Phys. Rev. E* **93**, 062317 (2016).

260. Narayan, O. & Saniee, I. Large-scale curvature of networks. *Phys. Rev. E* **84**, 066108 (2011).

261. Albert, R., DasGupta, B. & Mobasheri, N. Topological implications of negative curvature for biological and social networks. *Phys. Rev. E* **89**, 032811 (2014).

262. Borassi, M., Chessa, A. & Caldarelli, G. Hyperbolicity measures democracy in real-world networks. *Phys. Rev. E* **92**, 032812 (2015).

263. Tadić, B., Andjelković, M. & Melnik, R. Functional geometry of human connectomes. *Sci. Rep.* **9**, 12060 (2019).

264. Chatterjee, S. & Sloman, L. Average Gromov hyperbolicity and the Parisi ansatz. *Adv. Math* **376**, 107417 (2019).

265. Shang, Y. Lack of Gromov-hyperbolicity in small-world networks. *Cent. Eur. J. Math.* **10**, 1152–1158 (2012).

266. Shang, Y. Non-Hyperbolicity of random graphs with given expected degrees. *Stoch. Model.* **29**, 451–462 (2013).

267. Aktas, M. E., Akbas, E. & El Fatmaoui, A. Persistence homology of networks: methods and applications. *Appl. Netw. Sci.* **4**, 61 (2019).

268. Patania, A., Vaccarino, F. & Petri, G. Topological analysis of data. *EPJ Data Sci.* **6**, 7 (2017).

269. Giusti, C., Pastalkova, E., Curto, C. & Itskov, V. Clique topology reveals intrinsic geometric structure in neural correlations. *Proc. Natl Acad. Sci. USA* **112**, 13455–13460 (2015).

270. Otter, N., Porter, M. A., Tillmann, U., Grindrod, P. & Harrington, H. A. A roadmap for the computation of persistent homology. *EPJ Data Sci.* **6**, 17 (2017).

271. Battiston, F. et al. Networks beyond pairwise interactions: structure and dynamics. *Phys. Rep.* **874**, 1–92 (2020).

272. Song, C., Gallos, L. K., Havlin, S. & Makse, H. A. How to calculate the fractal dimension of a complex network: the box covering algorithm. *J. Stat. Mech. Theor. Exp.* **2007**, P03006 (2007).

273. Blondel, V. D., Guillaume, J.-L., Lambiotte, R. & Lefebvre, E. Fast unfolding of communities in large networks. *J. Stat. Mech. Theor. Exp.* **2008**, P10008 (2008).

Author contributions
The authors contributed equally to all aspects of the Review Article.

Competing interests
The authors declare no competing interests.

Publisher's note
Springer Nature remains neutral with regard to jurisdictional claims in published maps and institutional affiliations.